## Check for updates

#### CANCER

# Protumoral lipid droplet-loaded macrophages are enriched in human glioblastoma and can be therapeutically targeted

Valeria Governa<sup>1</sup>, Kelin Gonçalves de Oliveira<sup>1</sup>, Anna Bång-Rudenstam<sup>1</sup>, Svenja Offer<sup>2</sup>, Myriam Cerezo-Magaña<sup>1</sup>, Jiaxin Li<sup>1</sup>, Sarah Beyer<sup>1</sup>, Maria C. Johansson<sup>1</sup>, Ann-Sofie Månsson<sup>1</sup>, Charlotte Edvardsson<sup>1</sup>, Faris Durmo<sup>3</sup>, Emma Gustafsson<sup>1</sup>, Axel Boukredine<sup>1</sup>, Pauline Jeannot<sup>4</sup>, Katja Schmidt<sup>5</sup>, Emelie Gezelius<sup>1</sup>, Julien A. Menard<sup>1</sup>†, Raquel Garza<sup>6</sup>, Johan Jakobsson<sup>6</sup>, Therese de Neergaard<sup>7</sup>, Pia C. Sundgren<sup>3,8,9</sup>, Aliisa M. Tiihonen<sup>10</sup>, Hannu Haapasalo<sup>11</sup>, Kirsi J. Rautajoki<sup>10</sup>, Pontus Nordenfelt<sup>7</sup>, Anna Darabi<sup>12</sup>, Karin Forsberg-Nilsson<sup>13,14,15</sup>, Alexander Pietras<sup>4</sup>, Hugo Talbot<sup>1</sup>, Johan Bengzon<sup>16</sup>, Mattias Belting<sup>1,17</sup>\*

Glioblastoma presents a formidable clinical challenge because of its complex microenvironment. Here, we characterized tumor-associated foam cells (TAFs), a type of lipid droplet-loaded macrophage, in human glioblastoma. Through extensive analyses of patient tumors, together with in vitro and in vivo investigations, we found that TAFs exhibit distinct protumorigenic characteristics related to hypoxia, mesenchymal transition, angiogenesis, and impaired phagocytosis, and their presence correlates with worse outcomes for patients with glioma. We further demonstrated that TAF formation is facilitated by lipid scavenging from extracellular vesicles released by glioblastoma cells. We found that targeting key enzymes involved in lipid droplet formation, such as diacylglycerol *O*-acyltransferase or long-chain acyl-CoA synthetase, effectively disrupted TAF functionality. Together, these data highlight TAFs as a prominent immune cell population in glioblastoma and provide insights into their contribution to the tumor microenvironment. Disrupting lipid droplet formation to target TAFs may represent an avenue for future therapeutic development for glioblastoma.

#### Authors, some rights reserved; exclusive licensee American Association for the Advancement of Science. No claim to original U.S. Government Works

#### INTRODUCTION

Glioblastoma (GBM) is a lethal brain cancer characterized by severe hypoxia, vascular hyperproliferation, and abnormal metabolism. The standard of care for patients newly diagnosed with GBM is neurosurgical resection followed by adjuvant radiotherapy and temozolomide chemotherapy, but cancer recurrence and death are almost inevitable (1). GBM cells reprogram their tumor microenvironment

<sup>1</sup>Division of Oncology, Department of Clinical Sciences, Lund, Lund University, Lund 221 00, Sweden. <sup>2</sup> Joint Mass Spectrometry Center (JMSC) at Comprehensive Molecular Analytics, Helmholtz Zentrum München, Neuherberg 85764, Germany. <sup>3</sup>Division of Diagnostic Radiology, Department of Clinical Sciences, Lund, Lund University, Lund 221 00, Sweden. <sup>4</sup>Division of Translational Cancer Research, Department of Laboratory Medicine, Lund, Lund University, Lund 221 00, Sweden. <sup>5</sup>Infectious Diseases and Immunodeficiency Section, Department of Medicine 3, University Hospital Erlangen, Friedrich-Alexander-University Erlangen, Erlangen 91054, Germany. <sup>6</sup>Laboratory of Molecular Neurogenetics, Department of Experimental Medical Science, Wallenberg Neuroscience Center and Lund Stem Cell Center, Lund University, Lund 221 00, Sweden. <sup>7</sup>Division of Infection Medicine, Department of Clinical Sciences, Lund, Lund University, Lund 221 00, Sweden. <sup>8</sup>Lund Bioimaging Centre, Lund University, Lund 221 00, Sweden. <sup>9</sup>Department of Medical Imaging and Function, Skåne University Hospital, Lund 221 85, Sweden. <sup>10</sup>Prostate Cancer Research Center, Faculty of Medicine and Health Technology, Tampere University and Tays Cancer Center, Tampere University Hospital, Tampere 33101, Finland. <sup>11</sup>Fimlab Laboratories Ltd., Tampere University Hospital, Tampere 33101, Finland. <sup>12</sup>Division of Neurosurgery, Department of Clinical Sciences, Lund, Lund University, Lund 221 00, Sweden. <sup>13</sup>Department of Immunology, Genetics and Pathology, Uppsala University, Uppsala 751 85, Sweden. <sup>14</sup>Biodiscovery Institute, University of Nottingham, Nottingham NG7 2QL, UK. <sup>15</sup>Science for Life Laboratory, Uppsala 752 37, Sweden. <sup>16</sup>Division of Neurosurgery, Department of Clinical Sciences, Lund, Lund University Hospital, Lund 221 85, Sweden. <sup>17</sup>Department of Hematology, Oncology and Radiophysics, Skåne University Hospital, Lund 221 85, Sweden.

\*Corresponding author. Email: mattias.belting@med.lu.se †Present address: HØIBERG P/S, Adelgade 12, DK-1304 Copenhagen K, Denmark. (TME), evoking resistance to radiochemotherapy and a compromised antitumor immune response, which leaves few therapeutic options. Therefore, a better understanding of the interaction of cancer cells with surrounding stromal cells is critical for delineating and reprogramming the immunosuppressive TME (2, 3).

Although recent studies have elucidated how malignant cells in various cancers confer rewired lipid metabolism as an adaptive response to their hostile microenvironment (4-11), immune cell stress adaptation remains poorly understood. Major pathologies, including infectious and cardiovascular disease, feature lipid droplet (LD)-loaded macrophages, known as foam cells (12). LD accumulation in microglia has emerged as a hallmark of neurodegenerative disease and appears to increase in the aged brain (13, 14). Currently, lipid-targeting drugs from the cardiovascular field are being evaluated for repurposed treatment of several pathologies, including cancer.

In GBM, tumor-associated macrophages (TAMs), either peripheral bone marrow-derived macrophages (BMDMs) or brain-resident microglia, may represent up to 50% of stromal cells within the microenvironment, and their content is associated with enhanced tumor growth and poor patient survival (2). Several important studies have described the GBM immune microenvironment using single-cell RNA sequencing (scRNA-seq), delineating the transcriptional heterogeneity of the myeloid compartment across species and disease stages (15, 16). The realization of TAM complexity within the TME governed by the plasticity of these cells, has challenged the paradigm of the TAM M1 and M2 dichotomy. However, attempts to eradicate the entire macrophage population have failed as a therapeutic concept, highlighting the urgent need for additional strategies aimed at reversing tumor-promoting functions of TAMs (17–19).

Here, we identified an immune cell subset of CD68<sup>+</sup>LD<sup>+</sup> macrophages, or tumor-associated foam cells (TAFs), in samples from patients with GBM, reminiscent of the hallmark macrophage phenotype of atherosclerotic lesions. Comprehensive patient tumor profiling revealed a proangiogenic and antiphagocytic TAF signature associated with poorer patient outcome. Mechanistically, we found that the TAF phenotype could be conferred to macrophages by increased scavenging of glioma cell–derived extracellular vesicles (EVs) in the hypoxic tumor niche. Our data further suggest that TAFs can be targeted by LD-disruptive drugs that may represent a therapeutic approach for GBM.

#### **RESULTS**

#### Identification of TAFs in human GBM biopsies

We initially assessed the LD phenotype in the healthy human brain, in low-grade glioma [LGG, astrocytoma World Health Organization (WHO) grade 2], and in GBM (WHO grade 4). Whereas LD-positive areas were absent and modestly present in the healthy brain and LGG, respectively, we found abundant LDs in GBM tissue (Fig. 1A), which was corroborated by LD staining and flow cytometry analysis of patient-derived cultures from fresh surgical resections (Fig. 1B). We next hypothesized that not only glioma cells but also the immune cell compartment, constituting on average 5 to 10% (LGG) and 25 to 40% (GBM) of the total tumor cell population (Fig. 1C and fig. S1, A and B), could acquire the LD phenotype. CD45<sup>+</sup>LD<sup>+</sup> cells were abundant in GBM, whereas, as expected, few CD45<sup>+</sup>LD<sup>+</sup> cells were observed in LGG (Fig. 1D). By quantifying CD45<sup>-</sup>LD<sup>+</sup> and CD45<sup>+</sup>LD<sup>+</sup> areas in GBM, we found that about half of LD<sup>+</sup> cells were also CD45<sup>+</sup> (Fig. 1E). This provided evidence that the impact on lipid metabolism by the TME, as previously shown in malignant cells (20-22), may also entail a substantial fraction of infiltrating immune cells. Given that TAMs of different ontogeny (BMDMs and microglia) are predominant among immune cells in GBM (16), together with the fact that lipid-rich macrophages are pathognomonic of several disease conditions, and were recently described in other cancers (23, 24), we focused on the TAM subfraction. We demonstrate that TAMs, based on the pan-macrophage marker CD68 (25), on average make up approximately 65% of the total immune cell population in GBM, whereas tumor-infiltrating lymphocytes (TILs; CD45<sup>+</sup> CD3<sup>+</sup>) and tumor-associated neutrophils (TANs; CD45<sup>+</sup>CD66b<sup>+</sup>) represent only 10 to 15% (Fig. 1F). We found CD68<sup>+</sup>LD<sup>+</sup> cells to be prevalent in GBM cryosections (almost 40% of total CD68<sup>+</sup>) as compared with LGG (<10%) (Fig. 1G). Circulating peripheral blood mononuclear cells (PBMCs) from patients with GBM and microglia in normal brain samples did not exhibit the LD<sup>+</sup> phenotype, as visualized by high-resolution confocal imaging (fig. S1, C and D) and imaging flow cytometry (fig. S1, E and F). Further supporting that LD-loaded cells were TAMs, we observed CD204<sup>+</sup>LD<sup>+</sup> and CD163<sup>+</sup>LD<sup>+</sup> cells, markers associated with a protumorigenic TAM phenotype (18, 26) (fig. S1, G and H). Moreover, LD (HILPDA, DGAT1, GOS2, PLIN1, PLIN2, PLIN3, and SOAT1) and TAM (CD14, CD68, CD163, ITGAM, AIF1, and FCGR3A) gene signatures correlated in The Cancer Genome Atlas (TCGA) program and the Chinese Glioma Genome Atlas (CGGA) datasets (fig. S1I) (27, 28). Together, these data highlight the presence of TAFs in the GBM immune cell landscape.

## TAFs exhibit a transcriptome signature with protumorigenic features

To determine the transcriptional phenotype of TAFs, we next isolated CD68<sup>+</sup>LD<sup>+</sup> (TAF) and CD68<sup>+</sup>LD<sup>-</sup> (no-TAF) areas from two different patient cohorts (n = 3 and 5, respectively, in a total of eight patients) by laser capture microdissection (LCM) for RNA profiling (Fig. 2A). We demonstrated differences between TAF and CD68<sup>+</sup>LD<sup>-</sup> transcriptomes (Fig. 2B); TAFs were enriched in "hypoxia"-related genes (e.g., ADM, PDPN, THBS1, and VEGFA) and in genes involved in "lipid response" (e.g., ACAT2, CAV1, NAMPT, and VLDLR), as shown by pathway overrepresentation analysis and gene set enrichment analysis (GSEA) (Fig. 2, C and D). Moreover, in both patient cohorts, we consistently found several key genes implicated in "immune regulation" (e.g., CD163, CD163L1, FCGR2B, and TGFB2) and "matrix remodeling" (e.g., DSE, MMP7, PLAU, and PLAUR) (Fig. 2, E and F). We extracted a TAF signature of 54 genes on the basis of their consistent overexpression when compared with CD68<sup>+</sup>LD<sup>-</sup> areas in both cohorts; this signature incorporated genes associated with their phenotypic characteristics (lipid response) as well as genes previously implicated in TAM biology (table S1). We showed that enriched genes in TAFs overall correlated with CD68 expression in the TCGA and CGGA cohorts (Fig. 2E, lower row), supporting that a high-purity macrophage population was obtained by LCM for gene expression analysis. Moreover, the lack of LDs in patient and healthy donor PBMCs (fig. S1, C, E, and F), together with similar expression of TAF signature genes in patient versus healthy donor PBMCs (fig. S1J), suggests that the LDloaded phenotype was not intrinsic to circulating PBMCs.

GBM is highly heterogeneous, with several discernable anatomical compartments, including cellular tumor, leading edge, infiltrating tumor, hypoxic/pseudopalisading regions, and perivascular niches (29). Among the most up-regulated genes in TAFs, we recognized several that define the mesenchymal-like state of GBM macrophages (e.g., CD44, NAMPT, PLAUR, and VIM) (30), and GSEA confirmed that TAFs are enriched in genes responsible for epithelialto-mesenchymal transition as compared with no-TAFs (fig. S2A). Moreover, increased expression of TAF signature genes correlated with the mesenchymal GBM subtype in TCGA and CGGA datasets (Fig. 2G). The mesenchymal phenotype has been associated with hypoxic regulation (31), with no apparent overlap with typical M1- and M2-like macrophages (18). TAMs in hypoxic regions are known to be primarily BMDM derived (15), which we independently corroborated by costaining for CD68 (total TAMs), TMEM119 (microglia marker), and CAIX (hypoxia marker) (fig. S2B). Accordingly, the TAF signature included some of the most up-regulated genes in hypoxic versus nonhypoxic GBM macrophages (e.g., LDHA, S100A, SPP1, and VIM) previously identified by scRNA-seq (15) and was mainly associated with BMDMs rather than yolk sacderived microglia by GSEA (fig. S2C). We next costained GBM tumor sections for CD68 and LDs together with either CD49d (BMDM marker) or TMEM119. Our results show that approximately 80 and 20% of TAFs (CD68+LD+) were also positive for CD49d and TMEM119, respectively, further supporting that most TAFs are BMDMs (fig. S2D). We further showed that TAFs were associated with tumor areas displaying overexpression of GLUT1, which defines hypoxic regions in GBM (Fig. 2H), and are less abundant and only scattered in LGG (fig. S2E). We supported these observations with immunohistochemistry (IHC) analysis for GFAP (GBM cells)

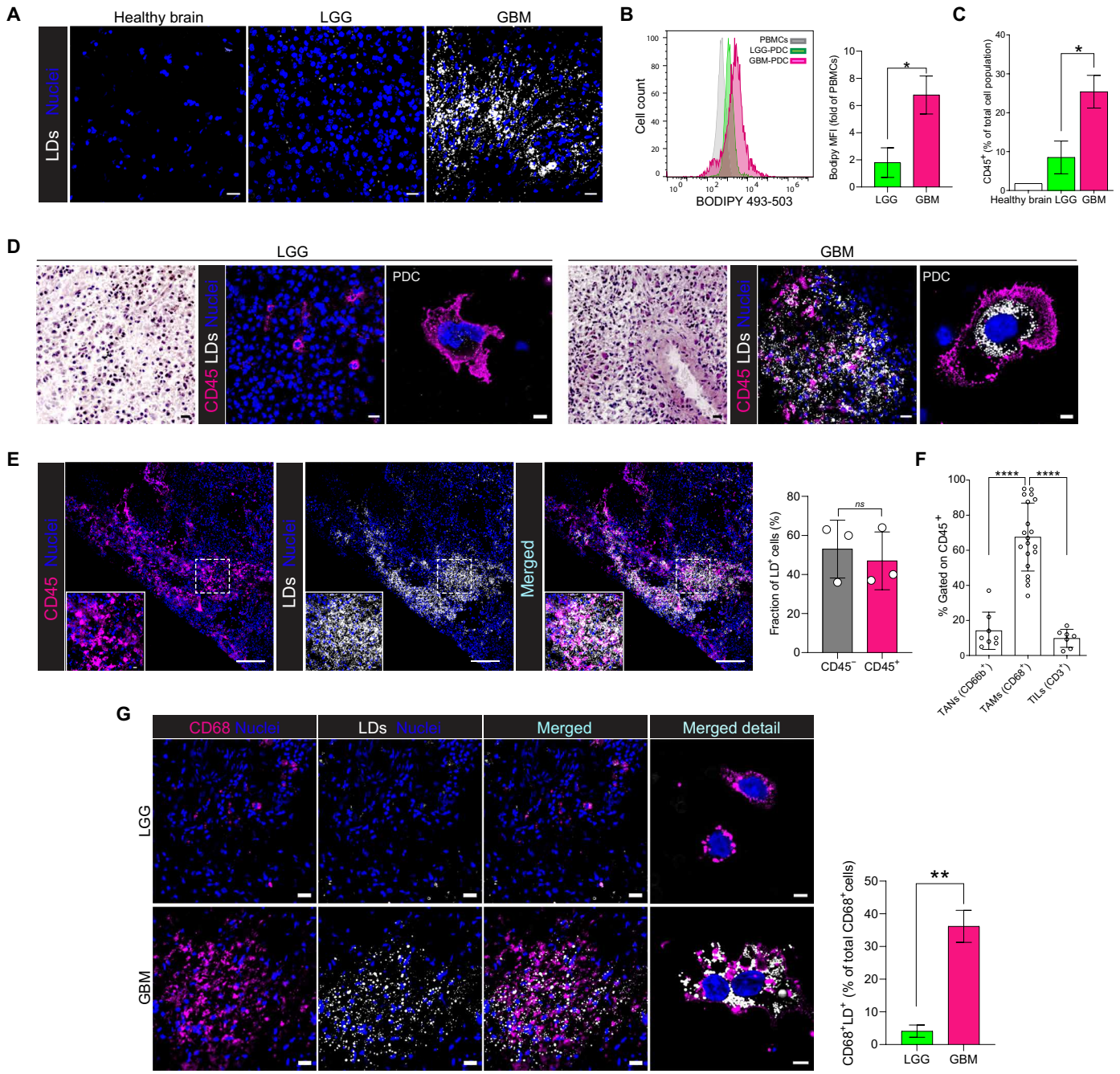


**Fig. 1. Identification of TAFs in human GBM. (A)** LipidTOX staining of LDs in the normal brain, LGG, and GBM. Nuclei were stained with Hoechst (images are representative of  $n \ge 5$  individuals per group). Scale bars, 20 μm. (**B**) Flow cytometry histogram (left) and quantification (right) of BODIPY-493-503 staining of GBM patient–derived culture (GBM-PDC) versus LGG-PDC, normalized against PBMCs (n = 4 individuals per group). MFI, mean fluorescence intensity. (**C**) Frequency of immune cells (CD45<sup>+</sup>) in GBM (n = 10), LGG (n = 4), and healthy brain (n = 1), assessed by flow cytometry (n = 15 samples in total). Statistical analysis by unpaired t test [(B) and (C)]. (**D**) H&E (left) and IF (middle and right) for CD45 and LDs in LGG and GBM tissue samples (scale bars, 20 μm) and in PDCs (scale bars, 5 μm). (**E**) IF staining of CD45<sup>+</sup>LD<sup>−</sup> and CD45<sup>+</sup>LD<sup>+</sup> in GBM (dashed squares, zoomed area) and corresponding quantification of the fraction of CD45<sup>+</sup> cells that were LD<sup>+</sup> (images are representative of n = 3 individuals, ≥7 areas per tumor). Statistical analysis by paired t test. Scale bars, 100 and 20 μm (inset). (**F**) Frequency of neutrophils (TANs), TAMs, and T cells (TILs) in GBM, assessed by flow cytometry ( $n = \ge 7$  individuals per group). Statistical analysis by one-way ANOVA with Tukey's correction for multiple comparisons. (**G**) IF images and corresponding quantification of the fraction of CD68<sup>+</sup>LD<sup>+</sup> of total CD68<sup>+</sup> cells in GBM and LGG (images are representative of n = 3 individuals per group, 53 areas per group). Statistical analysis by unpaired t test. Scale bars, 20 or 5 μm in merged detail. [(B), (C), and (E) to (G)] Data are presented as the mean  $\pm$  SEM. \*P < 0.005, \*P < 0.001, and \*\*\*\*P < 0.0001.

and CD68, which showed the presence of GFAP<sup>-</sup>CD68<sup>+</sup> areas with bright vacuoles in perinecrotic regions (Fig. 2I). To further address the BMDM versus microglia ontogeny, we next performed

single-nucleus RNA sequencing (snRNA-seq) on fresh frozen GBM tumor tissues (n = 16). In accordance with previous studies (32), we observed an underrepresented TAM cluster (fig. S3, A to C),

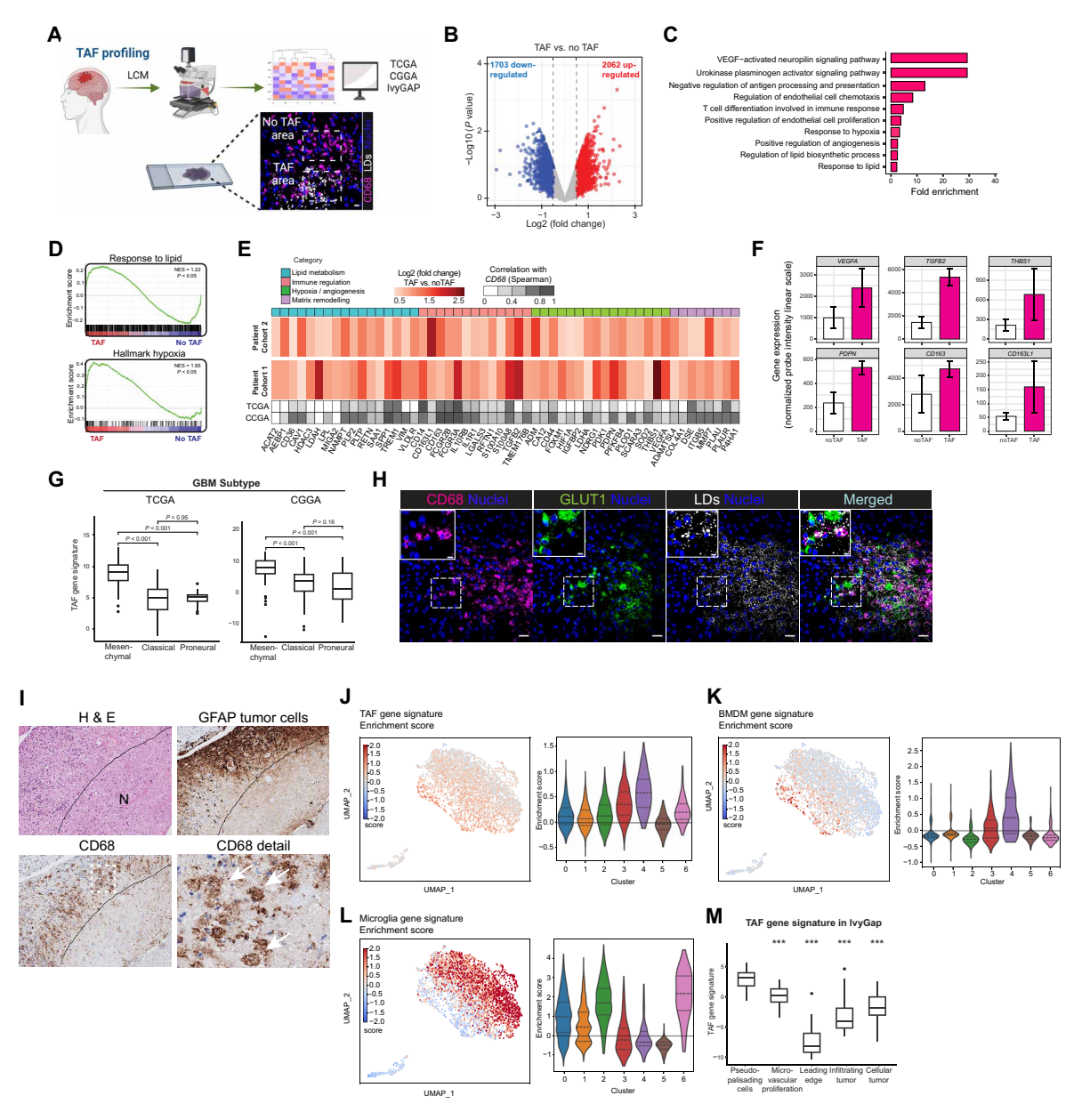


Fig. 2. TAFs exhibit a transcriptome signature with protumorigenic features and infiltrate the GBM hypoxic niche. (A) Schematic overview of TAF profiling in GBM by LCM and IF staining illustrating typical CD68<sup>+</sup>LD<sup>-</sup> (no-TAF) and CD68<sup>+</sup>LD<sup>+</sup> (TAF) areas (dashed white squares) captured by LCM from eight patients for comparative gene expression analysis. (B) Gene expression in TAF versus no-TAF areas ( $\log_2$  of fold change, x axis, versus statistical significance with P value as  $-\log_{10}$ , y axis). (C) Pathway analysis of up-regulated gene IDs (cutoff, 0.5 log<sub>2</sub> of fold change, P < 0.05) in TAF versus no-TAF areas, calculated via Fisher's exact test. (**D**) Significant enrichment of "response to lipid" and "hallmark hypoxia" genes in TAF versus no-TAF areas. (E) Up-regulated genes in TAF versus no-TAF regions from two separate patient cohorts (1 and 2), categorized into four groups (top row). Bottom rows show correlations between TAF signature genes and CD68 expression in the TCGA and CGGA datasets. Correlation of target genes with CD68 was performed with Spearman's R. (F) Expression of key genes involved in hypoxia/angiogenesis and immune regulation in TAF versus no-TAF samples. (G) Enrichment of the TAF gene signature across GBM subtypes in data from the TCGA and CGGA cohorts (TCGA: n = 131 primary GBM, IDH–wild type, n = 60, 48, 12, and 11 for the mesenchymal, classical, proneural, and unknown subtypes, respectively; CCGA: n = 183 primary GBM, IDH-wild type, n = 57, 69, 57, and 11 for the mesenchymal, classical, and proneural subtypes, respectively). Comparison of group means was performed with Wilcoxon signed-rank test. (H) Evaluation of TAF enrichment in the hypoxic GBM niche by IF staining for CD68, LDs, and GLUT1 (dashed squares, zoomed area). Scale bars, 20 and 5 μm (zoomed). Images are representative of n > 5 individual tumors. (I) H&E (upper left) of GBM tissue highlighting the necrotic area (N) and IHC for GFAP (tumor cells, upper right) and CD68 (lower images) in consecutive sections (dashed square, zoomed area; white arrows, vacuolated CD68 $^+$  cells). Images are representative of n=3 individual tumors. (J to L) snRNA-seq analysis of immune subclusters of GBM samples (n = 16 individuals), showing enrichment scores of the TAF gene signature (J), the BMDM gene signature (K), and the microglia gene signature (L) illustrated by Uniform Manifold Approximation and Projection (UMAP) (left). Violin plots (right) show enrichment scores per subcluster. The lines indicate the median and the first and third quartiles. (M) Quantification of TAF gene signature expression in the indicated GBM regions; data were retrieved from IvyGAP (n = 122). Comparison of group means versus "pseudo-palisading cells" was performed with the Wilcoxon signed-rank test. The box represents the interquartile range with the median value; the upper and lower quartiles are represented by whiskers, and outliers are represented as dots. \*\*\*P < 0.001.

probably due to loss during tissue or library processing. We demonstrated that the TAF signature preferentially associated with BMDM clusters compared with microglia clusters, particularly in two specific BMDM subclusters (3 and 4) (Fig. 2, J to L). This provides more direct evidence that TAFs are predominantly BMDMs. Last, interrogation of anatomical transcriptome data from the Ivy Glioblastoma Atlas Project (IvyGAP) (29) demonstrated that the TAF signature predominated in the hypoxic/pseudopalisading region, with a relatively limited contribution to the leading edge transcriptome (Fig. 2M). Together, these data indicate that TAFs primarily consist of BMDMs and are enriched within the hypoxic GBM niche. Moreover, gene profiling suggests that TAFs exhibit key protumorigenic features, such as angiogenesis, immune regulation, and matrix remodeling.

#### TAF abundance is associated with outcome in human GBM

The protumorigenic features of the TAF gene signature motivated us to investigate how TAF abundance correlates with tumor aggressiveness and patient outcome. We explored a possible association between TAFs and prognosis in a patient cohort with a broad survival range (80 to 1418 days), all receiving standard oncological treatment according to international guidelines (n = 36; table S2). Because most CD45<sup>+</sup>LD<sup>+</sup> cells were also CD68<sup>+</sup>LD<sup>+</sup> (Fig. 1), and given that CD45 provides a distinct and distinguishable surface signal in tissue sections, in contrast with the primarily cytoplasmic CD68, we used CD45 and LD costaining for scoring. For three representative TAFlow and TAFhigh cases, we observed variation in the TAF score (the fraction of CD45<sup>+</sup> cells that were LD<sup>+</sup>) among GBM tumors (Fig. 3A). By plotting survival and TAF scores as continuous variables in the entire cohort, we demonstrated a significant, inverse correlation between the TAF score and survival (r = -0.65; P = 0.0005) (Fig. 3B). Accordingly, Kaplan-Meier analysis with patients dichotomized according to TAF score showed that patients in the TAFlow group had a significantly improved survival probability as compared with those in the TAFhigh group (hazard ratio = 3.3; P = 0.002) (Fig. 3C). To understand whether these correlations were simply a reflection of the total tumor volume and degree of necrosis, we next analyzed contrast-enhanced T1-MRI images at presurgery (available from n = 13 patients) using whole tumor and necrosis segmentation (33). However, we observed no apparent correlations between the TAF score and tumor volume or the ratio of necrosis to tumor volume, respectively (fig. S4, A and B). Moreover, in both the TCGA and CGGA cohorts, we found that increased expression of TAF signature genes correlated with a higher glioma grade (Fig. 3, D and E, left panels), IDH-wild-type status (Fig. 3, D and E, right panels), and poorer survival (Fig. 3, F and G). We conclude that TAF abundance negatively correlated with patient outcome.

#### GBM-EVs fuel macrophage LD acquisition through hypoxia-induced lipid transfer that is reversible by DGAT1 and ACSL inhibition

We were next interested in understanding how TAMs may acquire the LD-loaded phenotype. Given that GBM tumors are poorly perfused and relatively inaccessible to a systemic supply of lipids and other nutrients, we explored a paracrine mechanism whereby glioma cells rewire macrophages into the LD phenotype. In this context, EVs constitute an attractive lipid source, and numerous reports have shown excessive EV release and uptake in response to tumor

hypoxia (34-36). We established an in vitro model of primary human macrophages differentiated from circulating CD14<sup>+</sup> cells (Fig. 4A), conditioned at oxygen-deprived conditions (1% O<sub>2</sub>) to mimic the hypoxic GBM environment. Initially, we elucidated how LD dynamics were affected by either whole conditioned media (CM) or only the EV fraction of freshly isolated cultures from patients with GBM. In both cases, we observed increased LD loading as compared with unconditioned, control medium (Fig. 4B). In addition, GBM cell-derived CM (GBM-CM) as well as GBM-EVs could induce a foamy phenotype comparable to LDL-treated primary macrophages (Fig. 4C). However, macrophages cultured in EV-depleted CM (supernatant, GBM-CM Sup) showed minimal LD loading, similarly to unconditioned medium (Fig. 4C). In the THP-1 macrophage cell line, we similarly found increased LD formation by GBM-CM and EVs but not EV-depleted supernatant (fig. S5A). The observed effects were not restricted to U87MG as EV donors, because CM and EVs from several primary GBM cultures likewise converted macrophages into foamy cells (fig. S5B; characterization of different EV sources is shown in fig. S5, C to H). Although hypoxia alone in unconditioned medium had no effect on LD abundance, we found increased LD loading in hypoxic as compared with normoxic macrophages when treated with GBM-CM (fig. S5I) and EVs (Fig. 4D and fig. S5J) as the lipid source. Moreover, we found that hypoxic macrophages were even more LD loaded by EVs derived from hypoxic as compared with normoxic GBM cells (fig. S5K), further suggesting a requirement for hypoxia in generating foamy cells. To understand whether the observed effects of EVs could be attributed to transfer of EV-associated LDs, we next investigated the time kinetics of EV uptake by macrophages, which reached saturation within 3 hours (fig. S5L). Concurrently, we assessed EV-dependent LD formation at different time points (6, 12, and 24 hours), finding a stronger LD phenotype at 24 hours as compared with 12 hours and only few LDs at 6 hours (fig. S5M). These data suggest that there was no direct transfer of preformed LDs carried by EVs. The presence of a fatty acid synthase (FASN) inhibitor did not affect EV-induced LD formation (Fig. 4E), indicating that LD formation primarily results from EV lipid uptake rather than from the induction of lipid synthesis. To investigate the processing of GBM-EV lipids into LD storage more directly, we used an EV-lipid transfer assay (34) and observed the transfer of the EV-derived lipid probe (BODIPY-FA) into LDs, demonstrated by its colocalization with LipidTOX in recipient macrophages (Fig. 4F). Using U87MG as an EV donor source, we observed transfer of the lipid probe from CM and EVs to LDs, whereas EV-depleted CM supernatant showed no transfer (fig. S5N). The preferential LD induction in hypoxic macrophages (Fig. 4D and fig. S5I) was supported by efficient internalization of PKH67 fluorophore-labeled GBM-EVs into hypoxic TAFs (Fig. 4G). Further, we linked increased EV-mediated LD induction in hypoxia to increased EV uptake activity in macrophages in hypoxic conditions, as visualized by confocal microscopy imaging and quantified by flow cytometry (Fig. 4H).

The exact mechanism of EV uptake remains to be unraveled; however, cell-surface heparan sulfate proteoglycans (PGs) have been shown to facilitate EV uptake by tumor cells (37), including in hypoxic glioma cells (34). To understand whether similar mechanisms operate in macrophages, we next analyzed EV uptake and LD formation in the presence of the heparan sulfate mimetic heparin in hypoxic macrophages, showing a dose-dependent inhibition of EV uptake (fig. S6, A and B) that was associated with reduced

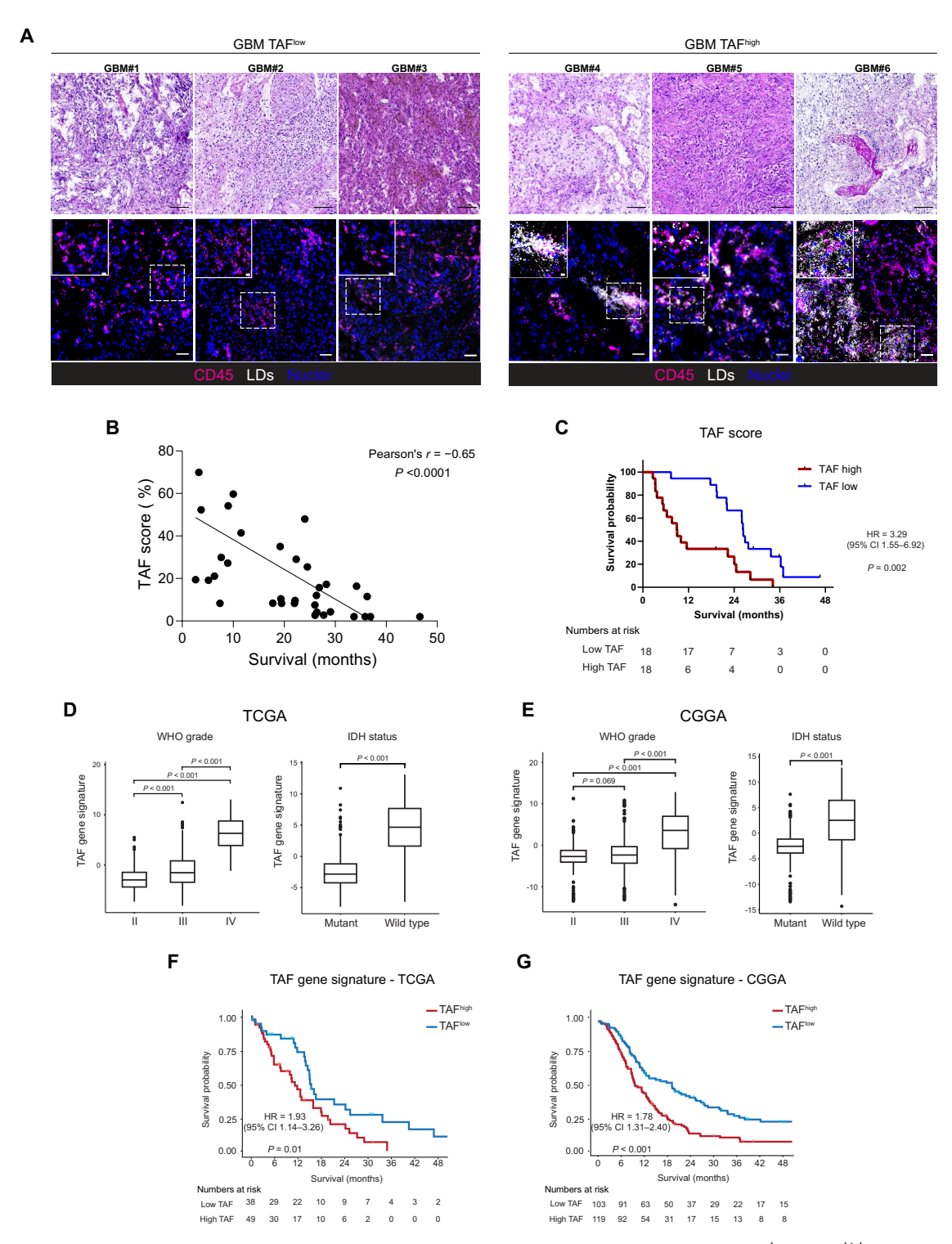


**Fig. 3. TAFs define a macrophage subset associated with outcome in human GBM.** (**A**) Representative H&E and IF of GBM TAF<sup>low</sup> and TAF<sup>high</sup> tumors. Scale bars, 100 μm (H&E), 50 μm (IF), and 10 μm (zoomed). (**B**) Shown is the correlation [determined by Pearson correlation (r)] between TAF score, defined as the fraction of CD45<sup>+</sup>LD<sup>+</sup> area versus total CD45<sup>+</sup> area (r = 36 individuals; ≥20 areas per patient), and survival. (**C**) Kaplan-Meier plot of survival against the TAF score dichotomized at the median. The log-rank (Mantel-Cox) test was performed. HR, hazard ratio; CI, confidence interval. (**D** and **E**) TAF gene signature expression across glioma grades (WHO 2, 3, and 4) and IDH status (mutant and wild type) in the TCGA (r = 669 individuals) (D) and CGGA (r = 651 individuals) (E) cohorts. Comparison of group means was performed with Wilcoxon signed-rank test. (**F** and **G**) Kaplan-Meier plot of survival data based on TAF gene signature expression in the TCGA (F) and CGGA (G) datasets. TAF<sup>low</sup> and TAF<sup>high</sup> correspond to patients in Q1 and Q4, respectively. Comparison of survival was performed with the log-rank test.

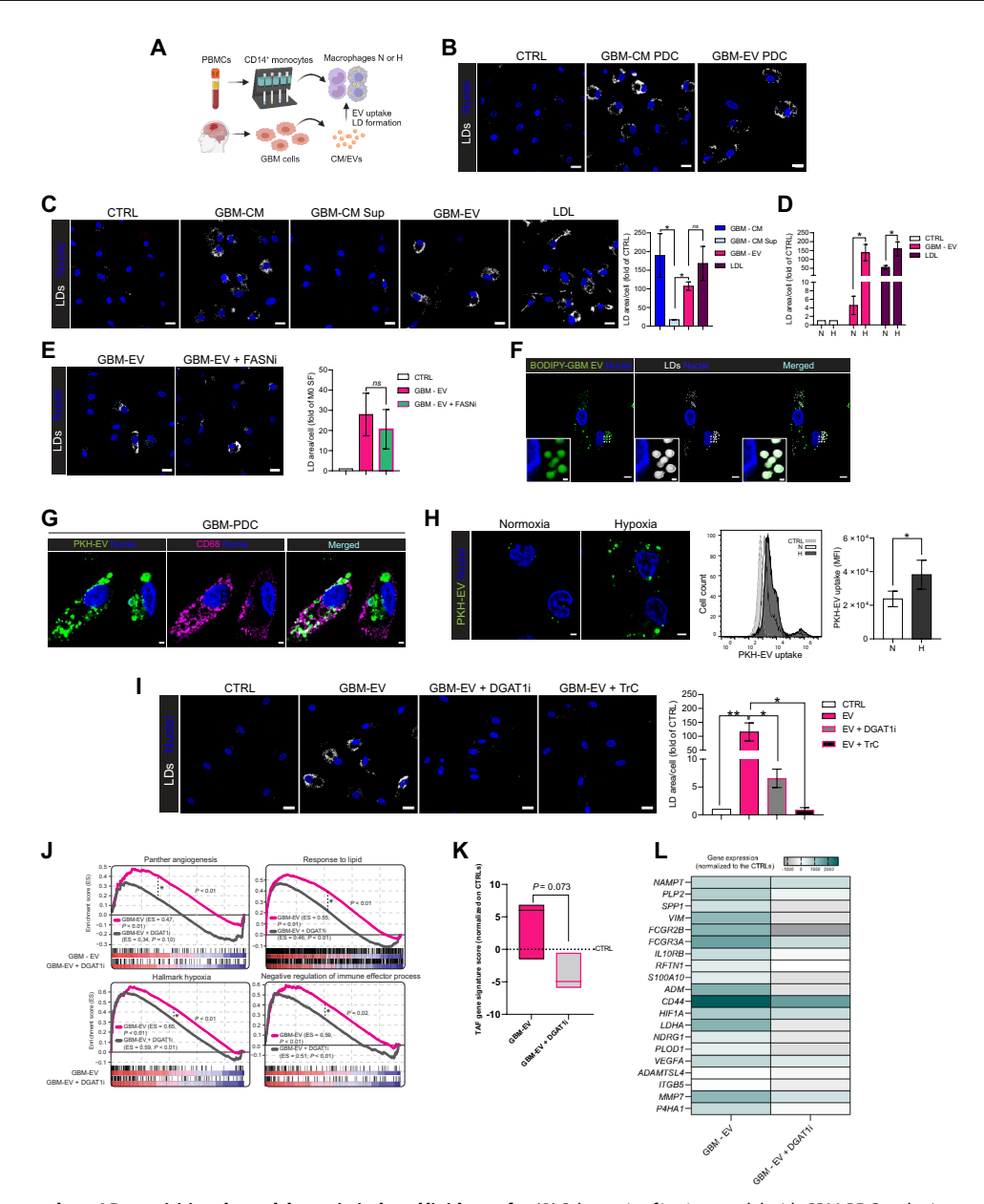


Fig. 4. GBM-EVs fuel macrophage LD acquisition through hypoxia-induced lipid transfer. (A) Schematic of in vitro model with GBM-PDC and primary macrophages. (B) Confocal microscopy of LD formation in hypoxic macrophages treated for 24 hours with whole CM or the EV fraction of CM (50 µg/ml) isolated from PDC. Scale bars, 20 µm. CTRL, control. Images are representative of n > 3 individual tumors per condition. (C) Confocal microscopy (left) and corresponding quantification of LD area per cell (right) in hypoxic macrophages, either untreated (CTRL) or treated for 24 hours with GBM-CM, EV-depleted CM [GBM-CM Sup (supernatant)], GBM-EV (50 µg/ml), or LDL (50 µg/ml). Scale bars, 20 µm. (D) LD area per cell after similar treatments as in (C) in normoxic (N) versus hypoxic (H) macrophages. For (C) and (D), n = 3 and 4 individual macrophage donors, respectively, and 18 to 24 images per condition, mean fold of CTRL ± SEM. Statistical analysis by one-way ANOVA with Tukey's correction for multiple comparisons. (E) Confocal microscopy visualization (left) and corresponding LD area per cell (right) in hypoxic macrophages, either untreated (CTRL) or treated for 24 hours with GBM-EV (50 μg/ml) in the absence or presence of FASN inhibitor (FASNi,  $100 \mu M$ ), n = 4 individual macrophage donors, mean  $\pm$  SEM. Statistical analysis via one-way ANOVA with Tukey's correction for multiple comparisons. Scale bars, 20 μm. (F) Transfer of GBM-EV-BODIPY-FAs into macrophage LDs (dashed white squares, zoomed area). Scale bars, 5 and 0.5 μm (zoomed). (G) High-resolution confocal microscopy of hypoxic GBM-PDC shows GBM-EV uptake (PKH67-EV) by CD68<sup>+</sup> cells (3 hours). Scale bar, 2 μm. Images are representative of n = 2 individual tumors. (H) Confocal microscopy (left), flow cytometry histogram (center), and quantification (right) of PKH67-EV (50  $\mu$ g/ml) uptake by normoxic (N) versus hypoxic (H) macrophages (n = 5 individual macrophage donors, mean ± SEM). Statistical analysis by paired t test. Scale bars, 2 µm. (I) Confocal microscopy (right) and corresponding quantification of LD area per cell (left) in hypoxic macrophages, either untreated (CTRL) or treated for 24 hours with GBM-EV (50  $\mu$ g/ml) in the absence or presence of DGAT1i (5  $\mu$ M) or TrC (0.5  $\mu$ M) ( $n \ge 3$  individual macrophage donors, mean  $\pm$  SEM). Statistical analysis via one-way ANOVA with Tukey's correction for multiple comparisons. Scale bars, 20 µm. (J) GSEA showing the enrichment of genes related to angiogenesis, response to lipids, hypoxia, and negative regulation of immune effector processes in hypoxic macrophages treated with GBM-EVs as compared with CTRL (magenta line), with or without DGAT1i treatment (GBM-EV + DGAT1i versus CTRL, gray line). (K) TAF gene signature expression in hypoxic macrophages treated with GBM-EV compared with macrophages treated with GBM-EV + DGAT1i, relative to CTRL (dashed line). Boxes represent the minimum and maximum TAF gene signature scores normalized to CTRLs with the median shown by the line inside the box. (L) Heatmap of TAF signature genes in hypoxic macrophages treated with GBM-EV or GBM-EV + DGAT1i. In (J) to (L), n = 3 separate experiments from one macrophage donor. In (K) and (L), the data were normalized to CTRL + DGAT1i. \*\*P < 0.005 and \*P < 0.05.

transformation into the foamy phenotype (fig. S6, C and D). These data were corroborated in THP-1 cells, showing dose-dependent inhibition of EV uptake (fig. S6, E and F) and EV-induced LD formation (fig. S6, G and H) by heparin treatment. Moreover, the PG transport pathway was induced in hypoxic macrophages, as shown by increased anti–heparan sulfate antibody uptake (fig. S6I).

Given that heparan sulfate PGs are ubiquitously expressed in the normal brain and thus less attractive for TAF-targeting purposes, we next explored drugs from the atherosclerosis field that were recently repurposed in preclinical tumor treatment studies (21, 38). LDs store large amounts of triglycerides, and we initially targeted diacylglycerol O-acyltransferase (DGAT1), which catalyzes the esterification of fatty acyl-coenzyme A (FA-CoA) with diacylglycerol (DAG), representing the key last step in triglyceride storage into LDs. We demonstrated that LD induction by LDL was prevented by the specific DGAT1 inhibitor (DGAT1i) A922500 in hypoxic macrophages (fig. S7A). As expected, CD68<sup>+</sup>LD<sup>+</sup> TAFs were abundant in cultures derived from patients with GBM (fig. S7B, t = 0 hours, lower row), and after 48 hours of conditioning in hypoxic, nutrient-poor medium, TAF LDs appeared to be consumed, whereas LD loading was strongly induced by GBM-CM and EVs (fig. S7B, t = 48 hours, lower row). The latter was true also for LGG cultures (fig. S7B, upper row), further suggesting that hypoxic stress in the presence of GBM-EVs is sufficient to convert LGG TAMs into the LD phenotype. We then attempted to inhibit CM and EV-dependent TAF induction with DGAT1i, showing a complete inhibition of LD formation in cultures from patients with GBM and LGG (fig. S7B). However, in two different mouse tumor settings with primary human GBM cells (fig. S7C), TAMs (F4/80<sup>+</sup>) only showed moderate LD accumulation (fig. S7D), reflecting the limitations of mouse models to fully reproduce TME complexity in patients (39). In the context of hypoxia and GBM-CM, however, mouse TAMs could also acquire LDs (fig. S7E). In the presence of DGAT1i, we observed few LDs in mouse TAMs (fig. S7E). DGAT1 inhibition prevented EV-dependent LD loading in hypoxic macrophages (Fig. 4I), and targeting of long-chain acyl-CoA synthetase (ACSL), which acts upstream of DGAT1, with triacsin C (TrC), likewise precluded LD formation by EVs (Fig. 4I) and GBM-CM (fig. S7F). These results further highlight that EV-induced LD formation depends on active processing by triglyceride biosynthetic enzymes rather than direct transfer of EV-incorporated LDs.

We next sought to understand how well in vitro generated, LDloaded macrophages could mimic the phenotype of patient TAFs. First, we showed that EV-induced LD formation in vitro recapitulated important features of patient TAFs, including the enrichment of genes associated with reinforced hypoxic, angiogenic, and immunodeficient functions and response to lipid, as compared with control (hypoxic macrophages that did not receive EVs), and these effects were attenuated by DGAT1 inhibition (Fig. 4J and fig. S7G). Moreover, most of the TAF signature genes were induced in LDloaded as compared with control macrophages (Fig. 4K and fig. S7H). A majority of these genes displayed reduced expression after DGAT1 inhibition to preclude LD formation (Fig. 4, K and L). Collectively, these results demonstrate that GBM-EVs can fuel macrophages to acquire LDs and key features of the TAF phenotype. This process is facilitated by the transfer of EV-associated lipids through a hypoxia-induced, heparan sulfate PG-dependent uptake route and can be prevented by inhibiting DGAT1 and ACSL.

### TAFs and LD-loaded macrophages exhibit impaired phagocytosis

Phagocytosis has a crucial role in the antitumor activity of TAMs through the elimination of malignant cells and initiation of adaptive immune responses. Impaired phagocytosis has emerged as a hallmark of LD-loaded microglia of the aging brain (13) and in foamy macrophages in the context of infectious disease (40). Moreover, decreased phagocytosis by lipid-laden TAMs was demonstrated in a murine model of gastric cancer (24). Overall, we found a reduction in expression of phagocytosis-related genes in TAFs compared with CD68<sup>+</sup>LD<sup>-</sup> (no-TAFs), as well as in GBM-EV-treated macrophages compared with untreated macrophages (Fig. 5A), whereas FcyRmediated phagocytosis showed no apparent difference (fig. S8A). In particular, the expression of the gene encoding the phagocytosisinhibitory Fc receptor FCGRIIB (41) was induced in patient TAFs compared with no-TAFs (Fig. 2E). FCGRIIB was also induced in GBM-EV-treated macrophages compared with untreated macrophages, an effect that was reversed by LD inhibition (Fig. 4L). As shown by Hussain et al. (42), FcyRIIb can be induced by hypoxia to suppress phagocytosis in macrophages. Moreover, transcription of the gene encoding FcyRIIb was shown to be directly driven by hypoxia-inducible factor 1α (HIF1α) and HIF2α, the master regulators of the hypoxic response (42). We observed that HIF1A mRNA was induced in patient TAFs compared with no-TAFs (Fig. 2E), as well as in GBM-EV-treated versus untreated macrophages, an effect that was attenuated by LD inhibition (Fig. 4L). Other studies (43) reported that lipid loading with fatty acids induces HIF1α, which was dependent on the PI3K-AKT-mTOR pathway, resulting in increased ACSL and LD formation in hepatocellular cancer cells. Moreover, lipid loading was shown to induce FcyRIIb in hepatocytes, and it was suggested that FcyRIIb, in addition to its negative regulation of phagocytosis, has a direct role in LD formation (44). We next hypothesized that GBM-EV lipid loading involves similar mechanisms by reinforcing the hypoxic HIF response in primary human macrophages. We found that p-AKT was induced in GBM-EV-treated macrophages (Fig. 5B) and that GBM-EVs increased mTOR activation (Fig. 5C) and protein abundance of HIF1α as well as FcγRIIb in hypoxic macrophages (Fig. 5D). Moreover, pharmacological induction of HIF with dimethyloxalylglycine (DMOG) in normoxic macrophages resulted in increased FcyRIIb expression (Fig. 5E). We found that pharmacological HIF stabilization resulted in EVinduced LD formation also in normoxic macrophages, an effect that was reversed by DGAT1 inhibition, thus mimicking the hypoxic situation (Fig. 5F).

We next studied the phagocytic capacity of TAFs and LD-loaded macrophages. Initially, we observed that TAFs appeared deficient in phagocytic uptake of pHrodo-conjugated particles (Fig. 5G). Moreover, the phagocytic activity in hypoxic macrophages was impaired by GBM-EV-induced LD loading, and pHrodo particle uptake was observed when LD formation was prevented by DGAT1 inhibition (Fig. 5H). Accordingly, the capacity to engulf and proteolytically process DQ-OVA antigen was decreased in LD-loaded macrophages (fig. S8B). This was consistent with previous studies showing impaired antigen cross-presentation in LD-loaded dendritic cells (23). Inspired by these data, we next set up a flow cytometry-based phagocytosis assay with macrophages to quantitatively assess the engulfment of pHrodo particles opsonized with human serum (fig. S8, C and D). Consistent with results from confocal microscopy imaging experiments, preconditioning with GBM-EVs

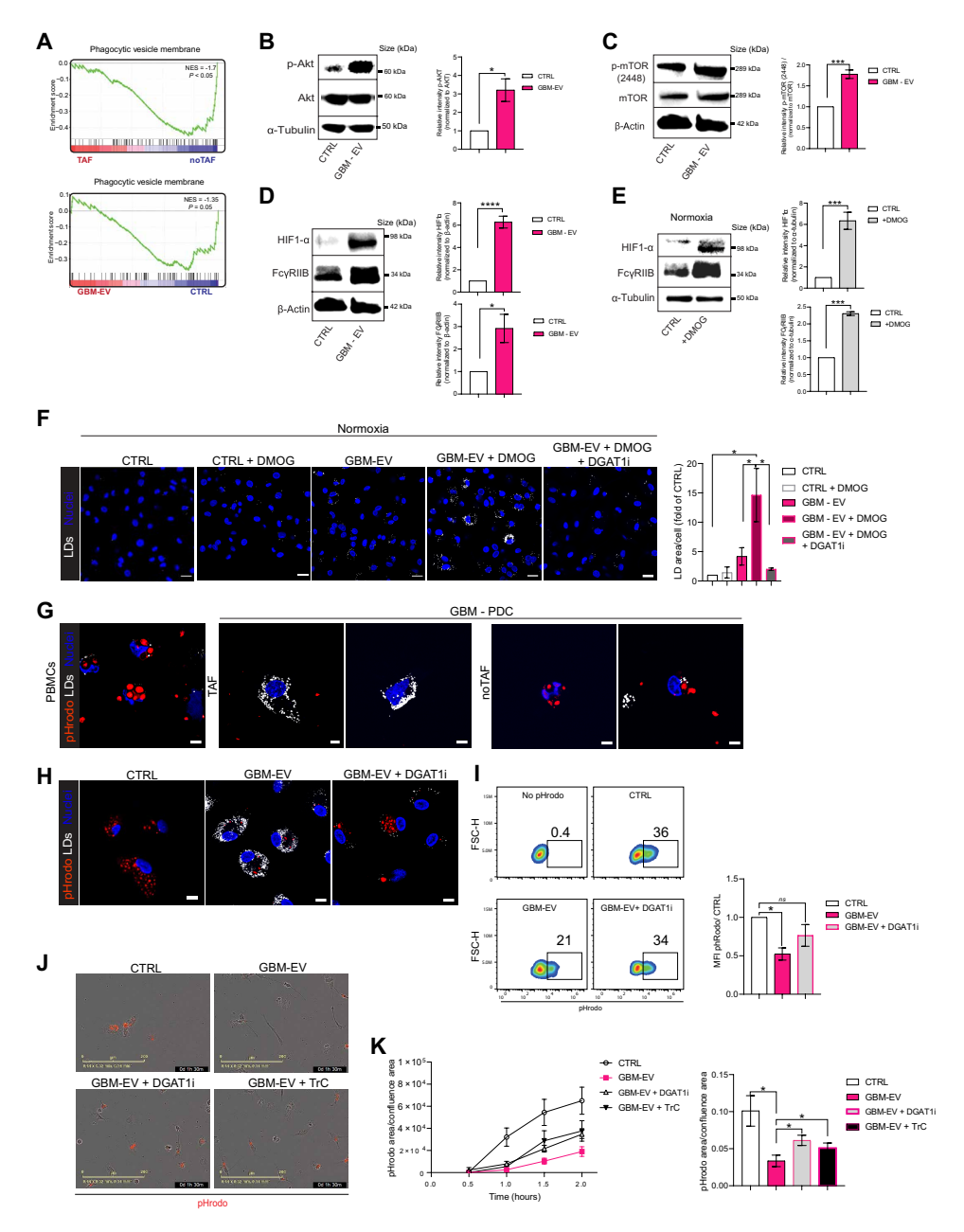


Fig. 5. TAFs and LD-loaded macrophages exhibit impaired phagocytosis. (A) GSEA shows depletion of phagocytosis-related genes in TAF versus no-TAF samples and in GBM-EV-treated versus untreated (CTRL) hypoxic macrophages. (B to D) Hypoxic macrophages treated with GBM-EVs or not (CTRL) were analyzed for phospho-AKT and total AKT (B), phospho-mTOR (Ser2448), total mTOR (C), and HIF1α and FCyRIIB (D) expression by Western blotting, with β-actin or α-tubulin as loading control. (E) HIF1α and FCyRIIB expression assessed via Western blot analysis in cell lysates from normoxic macrophages, either untreated (CTRL) or treated with DMOG (250 µM) for 24 hours. Right panels show corresponding semiguantifications by ImageJ normalized to loading control (fold of CTRL ± SEM). In (B) to (E), left panels show representative blots from n = 2 [(B) and (E)] and 3 [(C) and (D)] individual macrophage donors, with two replicates each. Statistical analysis by unpaired t test. (F) Confocal microscopy images and corresponding quantification of LD area per cell in normoxic macrophages, either untreated (CTRL) or treated for 24 hours with GBM-EV (50  $\mu$ g/ml) with or without DMOG and DGAT1i, as indicated ( $n \ge 3$  individual macrophage donors, fold of CTRL ± SEM). Scale bars, 20 μm. Statistical analysis was performed using one-way ANOVA with Tukey's correction for multiple comparisons. (G) Confocal microscopy shows deficient phagocytic uptake of pHrodo Red Zymosan BioParticles (2 hours) by TAFs isolated from GBM-PDC. PBMCs are shown as positive controls. Scale bars, 5 µm. Images are representative of n=3 individual tumors. (H) Similar experiment as in (G) measuring phagocytosis in LD-loaded macrophages preconditioned with GBM-EVs (GBM-EV) versus control macrophages (CTRL). GBM-EV preconditioned LD-loaded macrophages were treated or not with DGAT1i (5 μM). Scale bars, 10 μm. (I) Flow cytometry plot (left) of pHrodo particle uptake (ratio macrophage:pHrodo, 1:10) and corresponding quantification (right) in suspensions of CTRL, GBM-EV, and GBM-EV + DGAT1i-treated macrophages, as in (C) [n = 4 (CTRL and GBM-EV) and 2 (GBM-EV + DGAT1i) individual macrophage donors, mean ± SEM]. Statistical analysis via one-way ANOVA with Tukey's correction for multiple comparisons. (J and K) Phagocytosis of pHrodo particles was assessed by Incucyte live cell imaging of adherent CTRL macrophages and GBM-EV-, GBM-EV + DGAT1i-, or GBM-EV + triacsin C-treated (GBM-EV + TrC) macrophages. (J) Representative images at 1.5 hours of particle uptake. (K) Time-dependent phagocytosis (left) and quantification of particle uptake at 1.5 hours (right) (n = 2 individual macrophage donors with ≥3 technical replicates per group, mean ± SEM). Statistical analysis via one-way ANOVA with Tukey's correction for multiple comparison. \*\*\*\*P < 0.0001, \*\*\*P < 0.001, and \*P < 0.05.

was found to attenuate phagocytosis (approximately 50% of control), whereas GBM-EVs had no effect in the presence of DGAT1i (Fig. 5I). We corroborated these data by quantitative live imaging of adherent macrophages, demonstrating decreased phagocytosis in GBM-EV-treated as compared with control macrophages, and LD inhibition by targeting of DGAT1 or ACSL partially restored phagocytosis (Fig. 5, J and K). Together, these findings establish a functional link among GBM-EV transfer, LD formation, and decreased phagocytic capacity in macrophages.

## LD-loaded macrophages are associated with increased angiogenesis and tumor growth

With the aim to further decipher the functional relevance of TAFs, we decided to expand on the hypoxic and proangiogenic aspects of the patient TAF and LD-loaded macrophage gene signatures (Figs. 2 and 4J). Previous studies have shown a role of TAMs in the tumor angiogenic response (45–47). We next evaluated the correlation between vascular density and TAF and TAM abundance, respectively, by costaining for CD45, LD, and CD31. Tumor vascularization was greater in TAF<sup>high</sup> versus TAF<sup>low</sup> tumors (Fig. 6A), whereas we could not observe increased vascular density in TAMhigh versus TAMlow GBM tumors (fig. S8, E and F), which supports a link between TAF abundance and an increased angiogenic drive in GBM. Endothelial cell hyperproliferation is a hallmark of GBM, and the interaction between endothelial cells and TAMs has been shown to be critical for the development of aberrant blood vessels and tumor progression (45-47). We therefore next established an in vitro model with primary human brain-derived endothelial cells (HBMECs) to explore how GBM-CM or GBM-EVs may confer a proangiogenic phenotype to hypoxic macrophages (Fig. 6B). We verified that several angiogenesis-related TAF genes (CD44, THBS1, and VEGFA; Fig. 2, E and F) were also induced in LD-loaded macrophages preconditioned with GBM-EVs as compared with control (Fig. 6C; see also fig. S7H). Moreover, macrophages preconditioned with GBM-EVs showed increased secretion of key, proangiogenic cytokines and growth factors as compared with control (Fig. 6D). Our data consistently showed increased expression of vascular endothelial growth factor-A (VEGFA), one of the most potent proangiogenic factors, in TAFs and LD-loaded macrophages at both the gene and protein levels (Figs. 2, E and F, and 6, C and D), and this effect was reduced by LD inhibition (Fig. 6E). This was corroborated by enzyme-linked immunosorbent assay (ELISA), showing an approximately twofold increased release of VEGFA from LD-loaded macrophages as compared with control macrophages (Fig. 6F). Increased VEGFA secretion was reversed by inhibition of ACSL, whereas DGAT1 inhibition had no effect under these conditions, supporting that GBM-EV stimulation of macrophages may depend on LD formation (Fig. 6F). We next collected media derived from LD-loaded and control macrophages to assess the potential functional cross-talk between TAFs and HBMECs. We found that HBMECs cultured in medium from LD-loaded versus control macrophages exhibited increased ATP concentrations (approximately 1.5-fold; Fig. 6G) as well as increased migratory capacity (approximately 2-fold; Fig. 6H). Treatment of macrophages with DGAT1i to preclude LD formation attenuated the stimulatory effects on HBMECs (Fig. 6, H and I). Moreover, in support of a specific role for VEGFA, pretreatment of medium from LD-loaded macrophages with the VEGFAneutralizing antibody bevacizumab (Avastin) attenuated HBMEC activation (Fig. 6I).

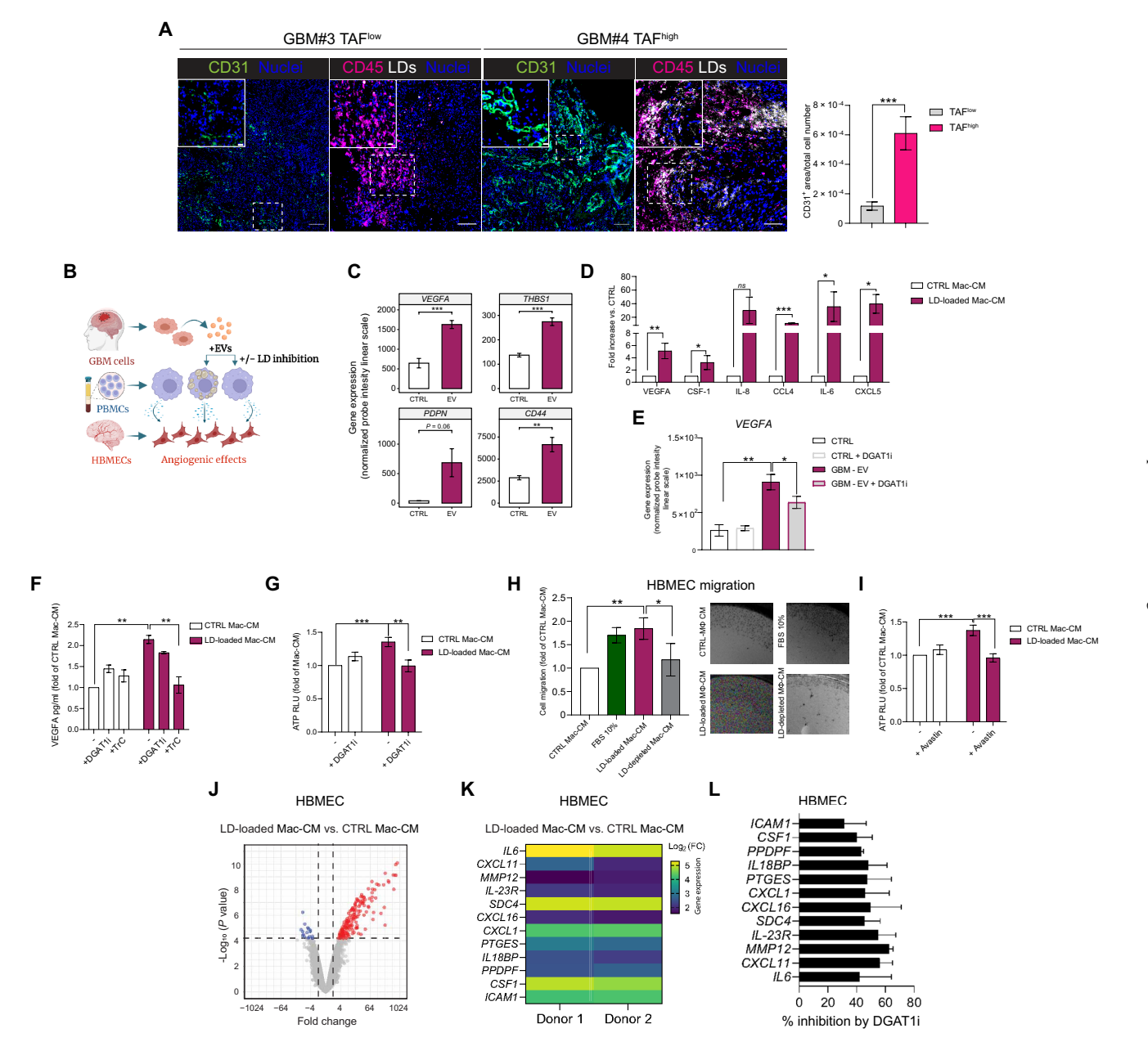
To further explore the macrophage-HBMEC cross-talk, we analyzed the HBMEC transcriptome after incubation with medium from control macrophages, LD-loaded macrophages, or macrophages treated with DGAT1i to deplete LDs. We observed upregulation of proangiogenic genes (e.g., *ICAM1*, *IL6*, and *SDC4*) in HBMECs incubated with medium from LD-loaded as compared with control macrophages (Fig. 6, J and K). Moreover, LD inhibition in macrophages by DGAT1i counteracted the proangiogenic activation of HBMECs (Fig. 6L), thus reinforcing that the GBM-macrophage-HBMEC signaling axis involves GBM-EV lipid transfer and LD induction in macrophages.

Last, we explored how these findings might be translated to the in vivo setting. As indicated, primary human GBM mouse models harbor few TAFs (fig. S7D). We then explored the presence of TAFs in a cell line-derived xenograft model (U87MG; fig. S9A), a patientderived xenograft model (U3054MG; fig. S9B), and a murine syngeneic model (GL261; fig. S9C), as well as in PDGFB- and shTrp53-induced murine GBM in fully immune-competent mice using the RCAS/tv-a system (fig. S9D). The RCAS/tv-a system was further used to generate postradiotherapy, recurrent GBM by subjecting symptomatic mice to 10 Gy radiotherapy and allowing tumors to recur before analysis (fig. S9D, right panel). In all models, we found no or only scarce TAFs. In lieu of a mouse model that could accurately mimic human GBM TAFs, we therefore coinjected U3054MG with human macrophages, preloaded (TAFs) or not (no-TAF) with GBM-EVs, or with TAFs treated with the LD inhibitor TrC (Fig. 7A). After 4 weeks of inoculation, tumors were replenished with the respective macrophage variants via repeated injection (Fig. 7A). To directly assess the biological effects of TAFs and LD inhibitor treatment, the experiment was terminated when the first mouse displayed neurological symptoms, as per the predetermined protocol. In support of a protumorigenic role of TAFs in mice, we demonstrated increased tumor growth in the presence of TAFs as compared with no-TAFs, an effect that was attenuated by LD depletion of TAFs with TrC (Fig. 7B). Immunofluorescence analysis of mouse tumor sections confirmed decreased LD loading in tumors provided with TAFs compared with LD-depleted TAFs (Fig. 7C). Moreover, we found that LD depletion of TAFs corresponded with reduced tumor angiogenesis, as suggested by decreased staining for CD31 (Fig. 7D). Together, these data suggest that TAFs play a crucial role in promoting angiogenesis in GBM through increased secretion of VEGFA, among other factors.

#### **DISCUSSION**

TAMs are prominent constituents of aggressive cancers, and an improved understanding of their specific phenotypic and functional traits may allow pharmacological targeting for clinical translation (2, 48). Here, we characterized TAFs, a subset of TAMs in human GBM featuring LD accumulation, which may represent a distinctive, targetable type of protumorigenic immune cell (fig. S10). As shown here and in previous studies (20–22, 34), GBM tumors are enriched in LD-positive areas that had primarily been attributed to malignant cells. However, we found that TAFs may constitute up to 40% of the total TAM population in human GBM.

Guo and colleagues recently showed that DGAT1 expression increases with glioma WHO grade and associates with poor survival in GBM; they also showed that oxidative stress and apoptosis are induced upon inhibition of DGAT1 in malignant cells (21).



 $\textbf{Fig. 6. TAFs and LD-loaded macrophages are associated with increased angiogenesis. (A)} \ Increased vascular density (CD31^+) in TAF^{high} (CD45^+LD^+) \ versus TAF^{low} (CD45^+LD^-) \$ GBM tumors, as shown by IF (left) and corresponding quantification (right). The white dashed line indicates zoomed area (n = 3 individual tumors per group and 5 or 6 areas per individual, mean  $\pm$  SEM). Statistical analysis via unpaired t test. Scale bars, 100 and 20  $\mu$ m (zoomed). (B) Schematic layout of GBM-macrophage-HBMEC cross-talk experiments. (C) Genes involved in angiogenesis induced in hypoxic macrophages treated with GBM-EVs versus CTRL (n = 5 individual macrophage donors). Statistical analysis via paired t test (VEGFA, THBS1, and CD44) and Wilcoxon signed-rank test (PDPN). (D) Immunoprofiling of CM from hypoxic macrophages preconditioned with GBM-CM (LD-loaded macrophage-CM) or with fresh medium (CTRL macrophage-CM). (E) VEGFA gene expression in hypoxic macrophages, either untreated (CTRL) or treated for 24 hours with GBM-EV (50 µg/ml) in the absence or presence of DGAT1i (5 μM). (F) ELISA of VEGFA in CTRL macrophage-CM and LD-loaded macrophage-CM with or without treatment with DGAT1i (5 μM) or TrC (0.5 µM). (G) Cell-titer assay (ATP measurement) of hypoxic HBMECs exposed to CM derived from macrophages preconditioned as in (F). RLU, relative light unit. (H) HBMEC transwell migration assay over 6 hours toward FBS (positive control), CTRL macrophage-CM, and LD-loaded macrophage-CM without or with DGAT1i (LD-depleted macrophage-CM). Quantification is shown on the left, and representative images are shown on the right. (I) Cell-titer assay of hypoxic HBMECs exposed to CTRL macrophage-CM or LD-loaded macrophage-CM for 72 hours in the absence (–) or presence of the VEGFA-blocking antibody avastin (1 µg/ml). [(D), (E), (H), and (I)] n = 3 and [(F) and (G)] n ≥ 3 individual macrophage donors per group. [(D) and (F) to (I)] Data are presented as the mean fold of CTRL ± SEM. Statistical analysis by unpaired t test (D) or by one-way ANOVA with Tukey's correction for multiple comparisons [(E) to (I)]. (J) Gene expression in HBMECs exposed over 6 hours to LD-loaded macrophage-CM as compared with CTRL macrophage-CM (log<sub>2</sub> of fold change versus statistical significance with P value as  $-\log_{10}$ , n=2 individual macrophage donors). (K) Heatmap shows selected, angiogenesis-related genes up-regulated in HBMECs exposed to LD-loaded macrophage-CM versus CTRL macrophage-CM from the experiment in (J). (L) CM from macrophages preconditioned with GBM-EVs or normal medium (CTRL) in the absence or presence of DGAT1i was added to HBMECs for 6 hours before gene expression analysis. Shown is the percentage of DGAT1i-dependent inhibition of the GBM-EV effect, mean  $\pm$  SEM, corrected for DGAT1 inhibition in the control condition. \*P < 0.05, \*\*P < 0.01, and \*\*\*P < 0.005.

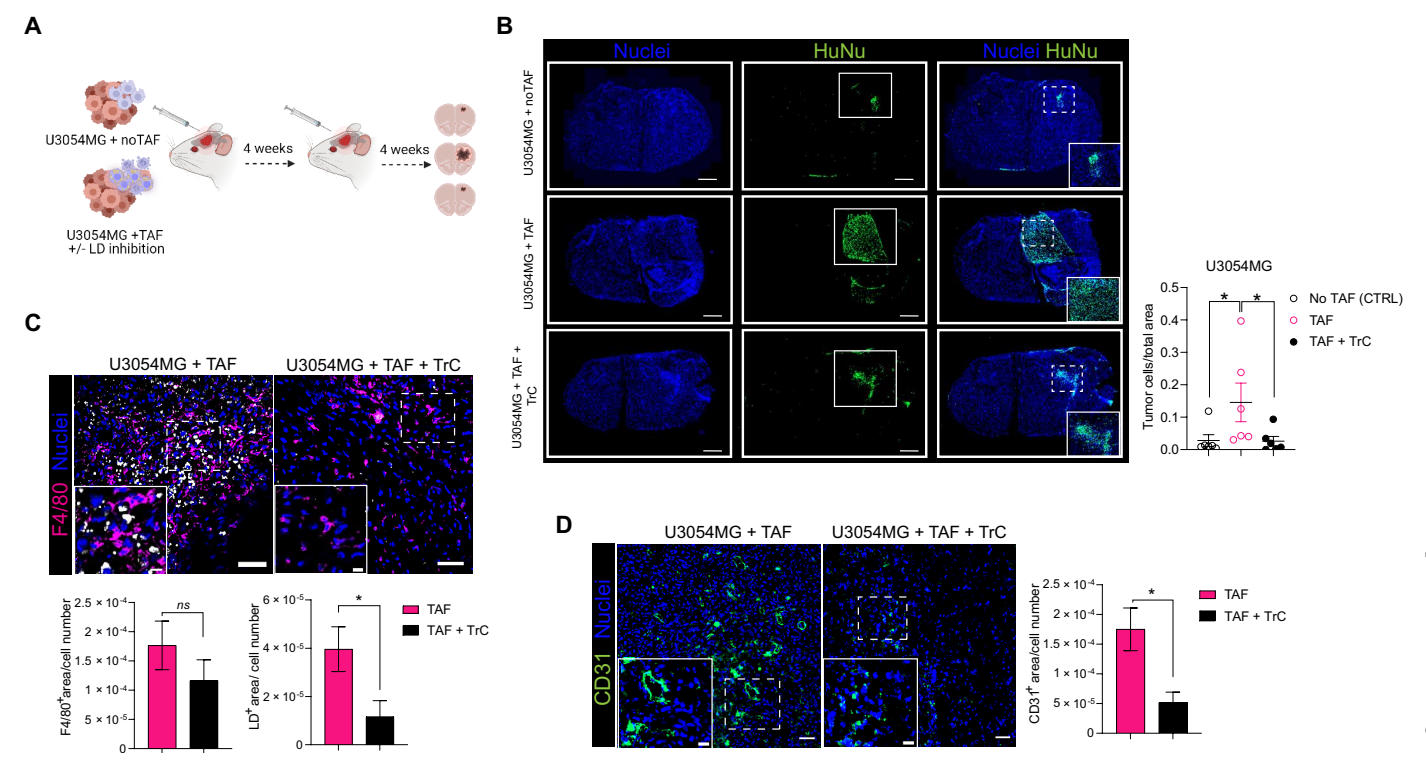


Fig. 7. The protumorigenic effects of TAFs are potentially targetable by LD inhibition. (A) Schematic of in vivo experiments. U3054MG cells were coinjected with macrophages, preloaded (TAF) or not (no-TAF) with GBM-EVs or with LD-depleted macrophages treated with the ACSCL inhibitor TrC (TAF + TrC) in NOD SCID mice. After 4 weeks, tumors were reconstituted with the respective macrophages, and mice were euthanized after another 4 weeks. (B) Representative IF for human cell nucleus antigen (HuNu) and corresponding quantification of tumor area (n = 6 mice per group, mean  $\pm$  SEM). Scale bars, 100 and 10  $\mu$ m (zoomed). (C and D) IF images and corresponding quantifications of (C) F4/80<sup>+</sup> mouse TAMs and LD<sup>+</sup> area and (D) vascular density (CD31<sup>+</sup>) (n = 3 mice per group and 5 or 6 areas per tumor, mean  $\pm$  SEM). Scale bars, 50 and 20  $\mu$ m (zoomed). \* $^{*}P < 0.05$ .

Moreover, pharmacological inhibition of DGAT1 suppressed GBM tumor growth and LD formation, as indicated by TIP47 staining, in a mouse flank model (21). However, LD loading in nonmalignant cells was not considered. DGAT1 inhibition has been tested in metabolic diseases in the clinic, and DGAT1 expression is low in the normal brain (21, 49). Thus, a dual rationale emerges for considering DGAT1 inhibition as a promising therapeutic strategy in GBM, targeting both malignant cells and protumorigenic TAFs.

Macrophage dysfunction by LD loading is a common phenomenon in major human conditions, including neurodegeneration, cancer, and atherosclerosis (13, 50-56). How TAMs acquire the LD phenotype in the TME, and its impact on cancer progression, remain an important area for further exploration. Our data suggest that EV lipids originating from GBM cells serve as substrates for LD formation, particularly in hypoxic macrophages. Yang et al. (56) showed that scavenger receptor CD36 can engulf fatty acids carried by EVs, resulting in tumor-promoting activities in liver metastasisassociated macrophages. Here, we suggest a role for hypoxiainduced, heparan sulfate PG-mediated uptake of GBM cell-derived EVs, resulting in increased LD formation. In GBM, previous studies have mostly focused on EV-mediated microRNA and protein transfer (57, 58). For example, GBM-EVs were shown to induce M2-like macrophage polarization by the transfer of interleukin-6 (IL-6) and miR-155-3p (59). Here, we show that the functional interaction with macrophages is driven in part by EV-mediated lipid transfer, given that reduced LD formation effectively mitigated the proangiogenic

and antiphagocytic TAF phenotype. It has been shown that tumorderived EV lipids cause dendritic cell dysfunction (60) and that adipocytes can feed macrophages with EV lipids, thereby regulating macrophage function in obesity (61). Moreover, LD loading was previously associated with dysfunctional natural killer (NK) cells that failed to control tumor growth in obese animals (62) and with exhausted CD8<sup>+</sup> T cells exhibiting impaired antitumoral functions (63). These findings, in conjunction with the present study, lay the foundation for future investigations on the broader role of EV lipid transfer to tumor-infiltrating immune cells, as well as on the respective contributions of microvesicles, exosomes, and the other EV species present in the TME (64).

Among potential mechanisms that may underlie the unfavorable prognostic association with TAFs, we demonstrated an association between LD loading and impaired phagocytic capacity. This is consistent with recent studies showing decreased phagocytosis in lipid-loaded macrophages in gastric and colorectal cancers (24). In the hypoxic TME, it is conceivable that macrophages build LD depots as a protective measure against toxic free FAs. Consequently, the energy supply from impaired FA oxidation may not suffice to execute efficient phagocytosis (65). In addition, lipids are critical in the transduction of phagocytic signals and in the remodeling of the actin cytoskeleton (66). Our studies propose an additional mechanism whereby EV-mediated LD loading may induce FcγRIIb by reinforcing the HIF response in hypoxic macrophages. Hypoxia-inducible lipid droplet associated (HILPDA), also known as a HIF responsive gene,

has been shown to promote LD formation in macrophages and cancer cells, partly by activating DGAT1 (67). Further studies should provide a more detailed mechanistic understanding of how lipid loading and a reinforced HIF response could regulate phagocytic activity in the TME. Our data further suggest that TAFs contribute to GBM malignancy through proangiogenic mechanisms involving HIF-induced VEGFA. BMDCs were shown to invade gliomas in response to hypoxia and stimulate neovascularization (68-70), but whether this phenomenon could be linked to TAM metabolic reprogramming was still unexplored. Our study demonstrates that TAFs and LD-loaded primary macrophages can exhibit robust proangiogenic characteristics, including increased VEGFA, to foster stimulatory cross-talk with HBMECs. Similarly, foam cell-driven angiogenesis in atherosclerosis is known to rely on increased VEGFA (71), indicating that LDs not only are passive storage organelles but also serve as signaling platforms for functions such as angiogenesis.

Our study has some important limitations, including the difficulty of sorting enough TAFs from clinical samples for downstream functional studies. Furthermore, the association between TAF abundance and poorer survival was based on a cohort from one study site that, however, was supported by independent analysis from the TCGA and CGGA cohorts. Yet, the concordance between patient tumor data and in vitro models using freshly isolated patientderived cultures and primary human cells provides reliable support for the concept that TAFs have clinical impact in GBM. The known limitations of murine GBM models, including less hypoxia, necrosis, and vascular proliferation (39), may explain the scarcity of endogenous TAFs across models. In support of this notion, mouse TAMs from human GBM xenografts also acquired LDs when put into hypoxia with GBM-CM ex vivo. We demonstrated increased tumor growth and an enhanced angiogenic response by introducing human TAFs into the mouse GBM microenvironment, an effect that was attenuated by inhibition of LD formation.

The urgent need for new therapeutic strategies has stimulated major efforts to not only target TAMs in GBM (72, 73) and other cancers, including inhibition of their recruitment and protumorigenic polarization, but also modulate their metabolic status (74). Despite promising studies in GBM, such as inhibition of the colony-stimulating factor-1 receptor (75, 76), this concept still awaits solid support by clinical studies. Hypothesizing that the several protumorigenic characteristics associated with TAMs may converge on their abnormal lipid phenotype, TAF depletion or reprogramming using LD inhibitors could offer a promising therapeutic avenue and serve as a viable alternative to other targeted treatments. To materialize this direction for GBM therapy, it will be critical to tailor LD-inhibiting agents with improved blood-brain barrier penetrance, allowing increased tumor bioavailability. Although such strategies could eradicate tumor cells, it may prove more beneficial to revert TAFs into antitumorigenic TAMs. In conclusion, we identify TAFs as a dominant, protumorigenic immune cell entity in human GBM and provide insights into the emerging role of immune cell lipid metabolism in cancer. Our results support efforts to develop LD-inhibiting drugs with the potential to modulate disease progression and patient outcome in GBM.

#### **MATERIALS AND METHODS**

#### Study design

The objective of this study was to molecularly characterize and investigate the protumorigenic role of TAFs in human GBM. We

hypothesized that the TAF phenotype can be conferred to macrophages by increased scavenging of glioma cell-derived EV lipids. We aimed to profile TAFs in patients with GBM using freshly resected tumor cultures and fresh frozen tissue. Human adult GBM tissue samples were obtained from patients referred to the Neurosurgery Department at Skåne University Hospital, Lund, Sweden. The inclusion criteria were age (18 years or above), WHO performance status (0 to 2), and the ability to comprehend and give written informed consent. The study was carried out according to the International Conference on Harmonization (ICH)/Good Clinical Practice (GCP) guidelines, in agreement with the Helsinki declaration, and approved by the local ethics committee, Lund University (Dnr. 2018/37). Clinical-pathological characteristics of included patients are provided in table S2. CD68<sup>+</sup>LD<sup>+</sup> (TAF) and CD68<sup>+</sup>LD<sup>-</sup> (no-TAF) areas were isolated by LCM from patients with GBM (n = 8) and analyzed for differential gene expression. The TAF gene signature was analyzed in a GBM tumor snRNA-seq dataset (n = 16) For survival analyses, we collected a cohort of patients with GBM (n = 36) with a broad survival range (80 to 1418 days; table S2). To reduce confounding biases, age distribution and MGMT promotor methylation status (established prognostic factors in GBM) were comparable in selected long-term and short-term survivors. To optimize reproducibility between scorers (blinded to clinical data), we decided to perform CD45 staining that provides a distinct surface signal as opposed to CD68. We then used in vitro models with as well as in publicly available TCGA, CGGA, and IvyGAP datasets. signal as opposed to CD68. We then used in vitro models with patient-derived cultures and primary GBM, macrophages, and HBMEC cultures, as well as established GBM and macrophage cell lines, to understand how TAFs acquire the LD phenotype and to explore TAF protumorigenic functions as well as the potential of TAF targeting as a therapeutic paradigm in GBM. Donor primary macrophage cultures with poor viability during differentiation were not used for experiments. No experimental data points were removed from the studies. Last, we interrogated the protumorigenic role of TAFs and possible therapeutic effects of LD inhibitors in vivo. For this purpose, we used NOD scid gamma (NSG) mice orthotopically injected with primary GBM cells and differentially preconditioned macrophages. In general, six animals were used for each treatment group. No power analyses were used to predetermine sample sizes, which instead were chosen on the basis of prior studies using comparable experimental paradigms. All experimental procedures were approved by the ethical committee for animal research in Malmö/Lund (ethical permit M144-14 and M145-14) and performed in accordance with the European Union animal rights and ethics directives.

#### Statistical analysis

Individual-level tabular data are presented in data file S1. GSEA statistics for the enrichment score (ES), normalized enrichment score (NES), nominal P value, and false discovery rate (FDR) were performed according to the GSEA software methodology (77). Significance of pathway overrepresentation terms was calculated according to Fisher's exact test. Significance tests of differentially expressed genes were performed on log<sub>2</sub>-transformed expression values (for which normality assumptions are applicable because of log-normal distribution) using moderated t statistics as per the limma package (78, 79). Correlation of TAF genes with CD68 (in TCGA and CCGA) was performed with Spearman's rank correlation rho test. snRNA-seq statistical analyses were performed as described in the Supplementary

Materials. Kaplan-Meier survival curves were generated using GraphPad Prism 9 (v 8.3.1; RRID:SCR 002798) and R (v 4.4.1; RRID:SCR 001905), and the log-rank test was performed to assess statistical significance between groups. For the TCGA and CGGA cohorts, differential survival significance and hazard ratios were assessed with the survival R package. Comparisons of subtype group (TCGA and CCGA) and tumor region (IvyGAP) means were performed with Wilcoxon signed-rank test. Statistical analyses of quantitative experimental models were performed using either paired or unpaired Student's t test (two-tailed), as indicated in the figure legends, with the Graph-Pad Prism 9 suite. Normal data distribution was analyzed using the Shapiro-Wilk test. Alternatively, one-way analysis of variance (ANOVA) was used with Tukey's correction for multiple comparisons. In vitro experiments were carried out with at least three independent biological experiments with separate patient cultures and macrophage donors or as indicated by n in the figure legends. Data are presented as means  $\pm$  SD or as means  $\pm$  SEM. All values with P < 0.05 were considered significant. All graphical illustrations were created with BioRender.com (RRID:SCR\_018361), and figure composition was performed with Adobe Illustrator 27.4 (RRID:-SCR\_010279).

#### **Supplementary Materials**

The PDF file includes: Materials and Methods Figs. S1 to S11 Tables S1 and S2 References (80–149)

Other Supplementary Material for this manuscript includes the following:

Data file S1 MDAR Reproducibility Checklist

#### **REFERENCES AND NOTES**

- K. Aldape, K. M. Brindle, L. Chesler, R. Chopra, A. Gajjar, M. R. Gilbert, N. Gottardo, D. H. Gutmann, D. Hargrave, E. C. Holland, D. T. W. Jones, J. A. Joyce, P. Kearns, M. W. Kieran, I. K. Mellinghoff, M. Merchant, S. M. Pfister, S. M. Pollard, V. Ramaswamy, J. N. Rich, G. W. Robinson, D. H. Rowitch, J. H. Sampson, M. D. Taylor, P. Workman, R. J. Gilbertson, Challenges to curing primary brain tumours. *Nat. Rev. Clin. Oncol.* 16, 509–520 (2019).
- J. Erbani, M. Boon, L. Akkari, Therapy-induced shaping of the glioblastoma microenvironment: Macrophages at play. Semin. Cancer Biol. 86, 41–56 (2022).
- M. L. Broekman, S. L. N. Maas, E. R. Abels, T. R. Mempel, A. M. Krichevsky, X. O. Breakefield, Multidimensional communication in the microenvirons of glioblastoma. *Nat. Rev. Neurol.* 14, 482–495 (2018).
- M. T. Accioly, P. Pacheco, C. M. Maya-Monteiro, N. Carrossini, B. K. Robbs, S. S. Oliveira, C. Kaufmann, J. A. Morgado-Diaz, P. T. Bozza, J. P. B. Viola, Lipid bodies are reservoirs of cyclooxygenase-2 and sites of prostaglandin-E2 synthesis in colon cancer cells. *Cancer Res.* 68, 1732–1740 (2008).
- W. Du, L. Zhang, A. Brett-Morris, B. Aguila, J. Kerner, C. L. Hoppel, M. Puchowicz, D. Serra, L. Herrero, B. I. Rini, S. Campbell, S. M. Welford, HIF drives lipid deposition and cancer in ccRCC via repression of fatty acid metabolism. *Nat. Commun.* 8, 1769 (2017).
- 6. C. Cheng, F. Geng, X. Cheng, D. Guo, Lipid metabolism reprogramming and its potential targets in cancer. *Cancer Commun.* **38**, 49–54 (2018).
- R. Mitra, T. T. Le, P. Gorjala, O. B. Goodman, Positive regulation of prostate cancer cell growth by lipid droplet forming and processing enzymes DGAT1 and ABHD5. BMC Cancer 17, 631 (2017).
- A. Pucer, V. Brglez, C. Payré, J. Pungerčar, G. Lambeau, T. Petan, Group X secreted phospholipase A2 induces lipid droplet formation and prolongs breast cancer cell survival. *Mol. Cancer* 12, 111 (2013).
- C. J. Sevinsky, F. Khan, L. Kokabee, A. Darehshouri, K. R. Maddipati, D. S. Conklin, NDRG1 regulates neutral lipid metabolism in breast cancer cells. *Breast Cancer Res.* 20, 55 (2018).
- Y. Sunami, A. Rebelo, J. Kleeff, Lipid metabolism and lipid droplets in pancreatic cancer and stellate cells. Cancer 10. 3 (2018).

- K. Yang, J. N. Rich, A delicate initiation: Lipolysis of lipid droplets fuels glioblastoma. Mol. Cell 81, 2686–2687 (2021).
- N. Krahmer, R. V. Farese, T. C. Walther, Balancing the fat: Lipid droplets and human disease. EMBO Mol. Med. 5, 973–983 (2013).
- J. Marschallinger, T. Iram, M. Zardeneta, S. E. Lee, B. Lehallier, M. S. Haney, J. V. Pluvinage, V. Mathur, O. Hahn, D. W. Morgens, J. Kim, J. Tevini, T. K. Felder, H. Wolinski, C. R. Bertozzi, M. C. Bassik, L. Aigner, T. Wyss-Coray, Lipid-droplet-accumulating microglia represent a dysfunctional and proinflammatory state in the aging brain. *Nat. Neurosci.* 23, 194–208 (2020)
- Y. Dong, V. W. Yong, Oxidized phospholipids as novel mediators of neurodegeneration. Trends Neurosci. 45, 419–429 (2022).
- A. R. Pombo Antunes, I. Scheyltjens, F. Lodi, J. Messiaen, A. Antoranz, J. Duerinck, D. Kancheva, L. Martens, K. De Vlaminck, H. Van Hove, S. S. Kjølner Hansen, F. M. Bosisio, K. Van der Borght, S. De Vleeschouwer, R. Sciot, L. Bouwens, M. Verfaillie, N. Vandamme, R. E. Vandenbroucke, O. De Wever, Y. Saeys, M. Guilliams, C. Gysemans, B. Neyns, F. De Smet, D. Lambrechts, J. A. Van Ginderachter, K. Movahedi, Single-cell profiling of myeloid cells in glioblastoma across species and disease stage reveals macrophage competition and specialization. *Nat. Neurosci.* 24, 595–610 (2021).
- F. Klemm, R. R. Maas, R. L. Bowman, M. Kornete, K. Soukup, S. Nassiri, J. P. Brouland, C. A. Iacobuzio-Donahue, C. Brennan, V. Tabar, P. H. Gutin, R. T. Daniel, M. E. Hegi, J. A. Joyce, Interrogation of the microenvironmental landscape in brain tumors reveals disease-specific alterations of immune cells. *Cell* 181, 1643–1660.e17 (2020).
- F. Khan, L. Pang, M. Dunterman, M. S. Lesniak, A. B. Heimberger, P. Chen, Macrophages and microglia in glioblastoma: Heterogeneity, plasticity, and therapy. J. Clin. Invest. 133, e163446 (2023).
- A. Mantovani, F. Marchesi, A. Malesci, L. Laghi, Tumor-associated macrophages as treatment targets in oncology. Nat. Rev. Clin. Oncol. 14, 399–416 (2018).
- S. Sarkar, A. Döring, F. J. Zemp, C. Silva, X. Lun, X. Wang, J. Kelly, W. Hader, M. Hamilton, P. Mercier, J. F. Dunn, D. Kinniburgh, N. Van Rooijen, S. Robbins, P. Forsyth, G. Cairncross, S. Weiss, V. W. Yong, Therapeutic activation of macrophages and microglia to suppress brain tumor-initiating cells. *Nat. Neurosci.* 17, 46–55 (2014).
- X. Wu, F. Geng, X. Cheng, Q. Guo, Y. Zhong, T. F. Cloughesy, W. H. Yong, A. Chakravarti, D. Guo, Lipid droplets maintain energy homeostasis and glioblastoma growth via autophagic release of stored fatty acids. iScience 23, 101569 (2020).
- X. Cheng, F. Geng, M. Pan, X. Wu, Y. Zhong, C. Wang, Z. Tian, C. Cheng, R. Zhang, V. Puduvalli, C. Horbinski, X. Mo, X. Han, A. Chakravarti, D. Guo, Targeting DGAT1 ameliorates glioblastoma by increasing fat catabolism and oxidative stress. *Cell Metab.* 32, 229–242.e8 (2020).
- S. Shakya, A. D. Gromovsky, J. S. Hale, A. M. Knudsen, B. Prager, L. C. Wallace,
   L. O. F. Penalva, H. A. Brown, B. W. Kristensen, J. N. Rich, J. D. Lathia, J. M. Brown,
   C. G. Hubert, Altered lipid metabolism marks glioblastoma stem and non-stem cells in separate tumor niches. *Acta Neuropathol. Commun.* 9, 101 (2021).
- D. L. Herber, W. Cao, Y. Nefedova, S. V. Novitskiy, S. Nagaraj, V. A. Tyurin, A. Corzo, H. I. Cho, E. Celis, B. Lennox, S. C. Knight, T. Padhya, T. V. McCaffrey, J. C. McCaffrey, S. Antonia, M. Fishman, R. L. Ferris, V. E. Kagan, D. I. Gabrilovich, Lipid accumulation and dendritic cell dysfunction in cancer. *Nat. Med.* 16, 880–886 (2010).
- Q. Luo, N. Zheng, L. Jiang, T. Wang, P. Zhang, Y. Liu, P. Zheng, W. Wang, G. Xie, L. Chen, D. Li, P. Dong, X. Yuan, L. Shen, Lipid accumulation in macrophages confers protumorigenic polarization and immunity in gastric cancer. *Cancer Sci.* 111, 4000–4011 (2020).
- D. Hambardzumyan, D. H. Gutmann, H. Kettenmann, The role of microglia and macrophages in glioma maintenance and progression. *Nat. Neurosci.* 19, 20–27 (2015).
- 26. A. Mantovani, P. Allavena, F. Marchesi, C. Garlanda, Macrophages as tools and targets in cancer therapy. *Nat. Rev. Drug Discov.* **21**, 799–820 (2022).
- Z. Zhao, K. N. Zhang, Q. Wang, G. Li, F. Zeng, Y. Zhang, F. Wu, R. Chai, Z. Wang, C. Zhang, W. Zhang, Z. Bao, T. Jiang, Chinese Glioma Genome Atlas (CGGA): A comprehensive resource with functional genomic data from Chinese glioma patients. *Genom. Proteom. Bioinform.* 19, 1–12 (2021).
- The Cancer Genome Atlas Research Network, J. N. Weinstein, E. A. Collisson, G. B. Mills, K. R. M. Shaw, B. A. Ozenberger, K. Ellrott, I. Shmulevich, C. Sander, J. M. Stuart, The cancer genome Atlas pan-cancer analysis project. *Nat. Genet.* 45, 1113–1120 (2013).
- R. B. Puchalski, N. Shah, J. Miller, R. Dalley, S. R. Nomura, J. G. Yoon, K. A. Smith, M. Lankerovich, D. Bertagnolli, K. Bickley, A. F. Boe, K. Brouner, S. Butler, S. Caldejon, M. Chapin, S. Datta, N. Dee, T. Desta, T. Dolbeare, N. Dotson, A. Ebbert, D. Feng, X. Feng, M. Fisher, G. Gee, J. Goldy, L. Gourley, B. W. Gregor, G. Gu, N. Hejazinia, J. Hohmann, P. Hothi, R. Howard, K. Joines, A. Kriedberg, L. Kuan, C. Lau, F. Lee, H. Lee, T. Lemon, F. Long, N. Mastan, E. Mott, C. Murthy, K. Ngo, E. Olson, M. Reding, Z. Riley, D. Rosen, D. Sandman, N. Shapovalova, C. R. Slaughterbeck, A. Sodt, G. Stockdale, A. Szafer, W. Wakeman, P. E. Wohnoutka, S. J. White, D. Marsh, R. C. Rostomily, L. Ng, C. Dang, A. Jones, B. Keogh, H. R. Gittleman, J. S. Barnholtz-Sloan, P. J. Cimino, M. S. Uppin, C. D. Keene, F. R. Farrokhi, J. D. Lathia, M. E. Berens, A. Iavarone, A. Bernard, E. Lein,

- J. W. Phillips, S. W. Rostad, C. Cobbs, M. J. Hawrylycz, G. D. Foltz, An anatomic transcriptional atlas of human glioblastoma. *Science* **360**, 660–663 (2018).
- T. Hara, R. Chanoch-Myers, N. D. Mathewson, C. Myskiw, L. Atta, L. Bussema, S. W. Eichhorn, A. C. Greenwald, G. S. Kinker, C. Rodman, L. N. Gonzalez Castro, H. Wakimoto, O. Rozenblatt-Rosen, X. Zhuang, J. Fan, T. Hunter, I. M. Verma, K. W. Wucherpfennig, A. Regev, M. L. Suvà, I. Tirosh, Interactions between cancer cells and immune cells drive transitions to mesenchymal-like states in glioblastoma. *Cancer Cell* 39, 779–792.e11 (2021).
- C. Neftel, J. Laffy, M. G. Filbin, T. Hara, M. E. Shore, G. J. Rahme, A. R. Richman,
   D. Silverbush, M. L. Shaw, C. M. Hebert, J. Dewitt, S. Gritsch, E. M. Perez,
   L. N. Gonzalez Castro, X. Lan, N. Druck, C. Rodman, D. Dionne, A. Kaplan, M. S. Bertalan,
   J. Small, K. Pelton, S. Becker, D. Bonal, Q. De Nguyen, R. L. Servis, J. M. Fung,
   R. Mylvaganam, L. Mayr, J. Gojo, C. Haberler, R. Geyeregger, T. Czech, I. Slavc, B. V. Nahed,
   W.T. Curry, B. S. Carter, H. Wakimoto, P. K. Brastianos, T. T. Batchelor,
   A. Stemmer-Rachamimov, M. Martinez-Lage, M. P. Frosch, I. Stamenkovic, N. Riggi,
   E. Rheinbay, M. Monje, O. Rozenblatt-Rosen, D. P. Cahill, A. P. Patel, T. Hunter, I. M. Verma,
   K. L. Ligon, D. N. Louis, A. Regev, B. E. Bernstein, I. Tirosh, M. L. Suvà, An integrative model of cellular states, plasticity, and genetics for glioblastoma. *Cell* 178, 835–849.e21 (2019).
- M. Slyper, C. B. M. Porter, O. Ashenberg, J. Waldman, E. Drokhlyansky, I. Wakiro, C. Smillie, G. Smith-Rosario, J. Wu, D. Dionne, S. Vigneau, J. Jané-Valbuena, T. L. Tickle, S. Napolitano, M. J. Su, A. G. Patel, A. Karlstrom, S. Gritsch, M. Nomura, A. Waghray, S. H. Gohil, A. M. Tsankov, L. Jerby-Arnon, O. Cohen, J. Klughammer, Y. Rosen, J. Gould, L. Nguyen, M. Hofree, P. J. Tramontozzi, B. Li, C. J. Wu, B. Izar, R. Haq, F. S. Hodi, C. H. Yoon, A. N. Hata, S. J. Baker, M. L. Suvà, R. Bueno, E. H. Stover, M. R. Clay, M. A. Dyer, N. B. Collins, U. A. Matulonis, N. Wagle, B. E. Johnson, A. Rotem, O. Rozenblatt-Rosen, A. Regev, A single-cell and single-nucleus RNA-Seq toolbox for fresh and frozen human tumors. Nat. Med. 26, 792–802 (2020).
- B. Driss, D. Cheban, Asymptotic stability of switching systems. Electron. J. Differ. Eq. 2010, 1–18 (2010).
- M. Cerezo-Magaña, H. C. Christianson, T. H. van Kuppevelt, K. Forsberg-Nilsson, M. Belting, Hypoxic induction of exosome uptake through proteoglycan-dependent endocytosis fuels the lipid droplet phenotype in glioma. *Mol. Cancer Res.* 19, 528–540 (2021).
- C. Shao, F. Yang, S. Miao, W. Liu, C. Wang, Y. Shu, H. Shen, Role of hypoxia-induced exosomes in tumor biology. *Mol. Cancer* 17, 120 (2018).
- K. Fraser, A. Jo, J. Giedt, C. Vinegoni, K. S. Yang, P. Peruzzi, E. A. Chiocca, X. O. Breakefield, H. Lee, R. Weissleder, Characterization of single microvesicles in plasma from glioblastoma patients. *Neuro-Oncology* 21, 606–615 (2019).
- H. C. Christianson, K. J. Svensson, T. H. van Kuppevelt, J.-P. Li, M. Belting, Cancer cell exosomes depend on cell-surface heparan sulfate proteoglycans for their internalization and functional activity. *Proc. Natl. Acad. Sci. U.S.A.* 110, 17380–17385 (2013).
- F. Nardi, O. E. Franco, P. Fitchev, A. Morales, R. E. Vickman, S. W. Hayward, S. E. Crawford, DGAT1 inhibitor suppresses prostate tumor growth and migration by regulating intracellular lipids and non-centrosomal MTOC protein GM130. Sci. Rep. 9, 3035 (2019).
- F. Akter, B. Simon, N. L. de Boer, N. Redjal, H. Wakimoto, K. Shah, Pre-clinical tumor models of primary brain tumors: Challenges and opportunities. *Biochim. Biophys. Acta Rev. Cancer* 1875, 188458 (2021).
- V. Guerrini, M. L. Gennaro, Foam cells: One size doesn't fit all. *Trends Immunol.* 40, 1163–1179 (2019).
- F. Nimmerjahn, J. V. Ravetch, Fc

  γ receptors as regulators of immune responses. Nat. Rev. Immunol. 8, 34–47 (2008).
- K. Hussain, R. Liu, R. C. G. Smith, K. T. J. Müller, M. Ghorbani, S. Macari, K. L. S. Cleary, R. J. Oldham, R. B. Foxall, S. James, S. G. Booth, T. Murray, L. N. Dahal, C. E. Hargreaves, R. S. Kemp, J. Longley, J. Douglas, H. Markham, S. J. Chee, R. J. Stopforth, A. Roghanian, M. J. Carter, C. H. Ottensmeier, B. Frendéus, R. I. Cutress, R. R. French, M. J. Glennie, J. C. Strefford, S. M. Thirdborough, S. A. Beers, M. S. Cragg, HIF activation enhances FcyRIIb expression on mononuclear phagocytes impeding tumor targeting antibody immunotherapy. J. Exp. Clin. Cancer Res. 41, 131 (2022).
- J. Seo, D. W. Jeong, J. W. Park, K. W. Lee, J. Fukuda, Y. S. Chun, Fatty-acid-induced FABP5/ HIF-1 reprograms lipid metabolism and enhances the proliferation of liver cancer cells. Commun. Biol. 3, 638 (2020).
- T. Shu, X. Song, X. Cui, W. Ge, R. Gao, J. Wang, Fc gamma receptor IIb expressed in hepatocytes promotes lipid accumulation and gluconeogenesis. *Int. J. Mol. Sci.* 19, 2932 (2018).
- M. Wenes, M. Shang, M. Di Matteo, J. Goveia, R. Martín-Pérez, J. Serneels, H. Prenen,
   B. Ghesquière, P. Carmeliet, M. Mazzone, Macrophage metabolism controls tumor blood vessel morphogenesis and metastasis. *Cell Metab.* 24, 701–715 (2016).
- I. Larionova, E. Kazakova, T. Gerashchenko, J. Kzhyshkowska, New angiogenic regulators produced by tams: Perspective for targeting tumor angiogenesis. Cancer 13, 3253–3240 (2021).
- 47. M. Mazzone, G. Bergers, Regulation of blood and lymphatic vessels by immune cells in tumors and metastasis. *Annu. Rev. Physiol.* **81**, 535–560 (2019).

- M. Russo, C. Nastasi, Targeting the tumor microenvironment: A close up of tumorassociated macrophages and neutrophils. Front. Oncol. 12, 871513 (2022).
- R. Naik, B. W. Obiang-Obounou, M. Kim, Y. Choi, H. S. Lee, K. Lee, Therapeutic strategies for metabolic diseases: Small-molecule diacylglycerol acyltransferase (DGAT) inhibitors. *ChemMedChem* 9, 2410–2424 (2014).
- M. Lee-Rueckert, J. Lappalainen, P. T. Kovanen, J. C. Escola-Gil, Lipid-laden macrophages and inflammation in atherosclerosis and cancer: An integrative view. Front. Cardiovasc. Med. 9, 777822 (2022).
- M. H. den Brok, T. K. Raaijmakers, E. Collado-Camps, G. J. Adema, Lipid droplets as immune modulators in myeloid cells. *Trends Immunol.* 39, 380–392 (2018).
- P. Li, M. Lu, J. Shi, Z. Gong, L. Hua, Q. Li, B. Lim, X. H. F. Zhang, X. Chen, S. Li, L. D. Shultz, G. Ren, Lung mesenchymal cells elicit lipid storage in neutrophils that fuel breast cancer lung metastasis. *Nat. Immunol.* 21, 1444–1455 (2020).
- M. Masetti, R. Carriero, F. Portale, G. Marelli, N. Morina, M. Pandini, M. Iovino, B. Partini, M. Erreni, A. Ponzetta, E. Magrini, P. Colombo, G. Elefante, F. Simone Colombo, J. M. M. den Haan, C. Peano, J. Cibella, A. Termanini, P. Kunderfranco, J. Brummelman, M. W. H. Chung, M. Lazzeri, R. Hurle, P. Casale, E. Lugli, R. A. DePinho, S. Mukhopadhyay, S. Gordon, D. Di Mitri, Lipid-loaded tumor-associated macrophages sustain tumor growth and invasiveness in prostate cancer. J. Exp. Med. 219, e20210564 (2021).
- R. Sun, R. Han, C. McCornack, S. Khan, G. T. Tabor, Y. Chen, J. Hou, H. Jiang, K. M. Schoch, D. D. Mao, R. Cleary, A. Yang, Q. Liu, J. Luo, A. Petti, T. M. Miller, J. D. Ulrich, D. M. Holtzman, A. H. Kim, TREM2 inhibition triggers antitumor cell activity of myeloid cells in glioblastoma. Sci. Adv. 9. eade3559 (2023).
- E. Timperi, P. Gueguen, M. Molgora, I. Magagna, Y. Kieffer, S. Lopez-Lastra, P. Sirven,
   L. G. Baudrin, S. Baulande, A. Nicolas, G. Champenois, D. Meseure, A. Vincent-Salomon,
   A. Tardivon, E. Laas, V. Soumelis, M. Colonna, F. Mechta-Grigoriou, S. Amigorena,
   E. Romano, Lipid-associated macrophages are induced by cancer-associated fibroblasts
   and mediate immune suppression in breast cancer. Cancer Res. 82, 3291–3306 (2022).
- P. Yang, H. Qin, Y. Li, A. Xiao, E. Zheng, H. Zeng, C. Su, X. Luo, Q. Lu, M. Liao, L. Zhao, L. Wei, Z. Varghese, J. F. Moorhead, Y. Chen, X. Z. Ruan, CD36-mediated metabolic crosstalk between tumor cells and macrophages affects liver metastasis. *Nat. Commun.* 13, 5782 (2022)
- K. E. Van Der Vos, E. R. Abels, X. Zhang, C. Lai, E. Carrizosa, D. Oakley, S. Prabhakar,
   O. Mardini, M. H. W. Crommentuijn, J. Skog, A. M. Krichevsky, A. Stemmer-Rachamimov,
   T. R. Mempel, J. El Khoury, S. E. Hickman, X. O. Breakefield, Directly visualized glioblastoma-derived extracellular vesicles transfer RNA to microglia/macrophages in the brain. Neuro-Oncology 18, 58–69 (2016).
- K. Al-Nedawi, B. Meehan, J. Micallef, V. Lhotak, L. May, A. Guha, J. Rak, Intercellular transfer of the oncogenic receptor EGFRvIII by microvesicles derived from tumour cells. Nat. Cell Biol. 10. 619–624 (2008).
- J. Xu, J. Zhang, Z. Zhang, Z. Gao, Y. Qi, W. Qiu, Z. Pan, Q. Guo, B. Li, S. Zhao, X. Guo, M. Qian, Z. Chen, S. Wang, X. Gao, S. Zhang, H. Wang, X. Guo, P. Zhang, R. Zhao, H. Xue, G. Li, Hypoxic glioma-derived exosomes promote M2-like macrophage polarization by enhancing autophagy induction. *Cell Death Dis.* 12, 1–16 (2021).
- X. Yin, W. Zeng, B. Wu, L. Wang, Z. Wang, H. Tian, L. Wang, Y. Jiang, R. Clay, X. Wei, Y. Qin,
   F. Zhang, C. Zhang, L. Jin, W. Liang, PPARα inhibition overcomes tumor-derived exosomal lipid-induced dendritic cell dysfunction. *Cell Rep.* 33, 108278 (2020).
- S. E. Flaherty, A. Grijalva, X. Xu, E. Ables, A. Nomani, A. W. Ferrante, A lipase-independent pathway of lipid release and immune modulation by adipocytes. *Science* 363, 989–993 (2019).
- X. Michelet, L. Dyck, A. Hogan, R. M. Loftus, D. Duquette, K. Wei, S. Beyaz, A. Tavakkoli, C. Foley, R. Donnelly, C. O'Farrelly, M. Raverdeau, A. Vernon, W. Pettee, D. O'Shea, B. S. Nikolajczyk, K. H. G. Mills, M. B. Brenner, D. Finlay, L. Lynch, Metabolic reprogramming of natural killer cells in obesity limits antitumor responses. *Nat. Immunol.* 19, 1330–1340 (2018).
- X. Liu, C. L. Hartman, L. Li, C. J. Albert, F. Si, A. Gao, L. Huang, Y. Zhao, W. Lin, E. C. Hsueh, L. Shen, Q. Shao, D. F. Hoft, D. A. Ford, G. Peng, Reprogramming lipid metabolism prevents effector T cell senescence and enhances tumor immunotherapy. Sci. Transl. Med. 13, eaaz6314 (2021).
- E. I. Buzas, The roles of extracellular vesicles in the immune system. Nat. Rev. Immunol. 23, 236–250 (2023).
- P. Calle, A. Muñoz, A. Sola, G. Hotter, CPT1a gene expression reverses the inflammatory and anti-phagocytic effect of 7-ketocholesterol in RAW264.7 macrophages. *Lipids Health Dis.* 18, 215 (2019).
- J. Yan, T. Horng, Lipid metabolism in regulation of macrophage functions. *Trends Cell Biol.* 30, 979–989 (2020).
- M. A. de la Rosa Rodriguez, S. Kersten, Regulation of lipid droplet homeostasis by hypoxia inducible lipid droplet associated HILPDA. *Biochim. Biophys. Acta Mol. Cell Biol. Lipids* 1865. 158738 (2020).
- M. De Palma, C. Murdoch, M. A. Venneri, L. Naldini, C. E. Lewis, Tie2-expressing monocytes: Regulation of tumor angiogenesis and therapeutic implications. *Trends Immunol.* 28, 519–524 (2007).

- C. Murdoch, M. Muthana, S. B. Coffelt, C. E. Lewis, The role of myeloid cells in the promotion of tumour angiogenesis. *Nat. Rev. Cancer* 8, 618–631 (2008).
- J. P. Greenfield, W. S. Cobb, D. Lyden, Resisting arrest: A switch from angiogenesis to vasculogenesis in recurrent malignant gliomas. *J. Clin. Invest.* 120, 663–667 (2010).
- P. Libby, P. M. Ridker, A. Maseri, Inflammation and atherosclerosis. Circulation 105, 1135–1143 (2002).
- P. Schmassmann, J. Roux, A. Buck, N. Tatari, S. Hogan, J. Wang, N. Rodrigues Mantuano, R. Wieboldt, S. Lee, B. Snijder, D. Kaymak, T. A. Martins, M. F. Ritz, T. Shekarian, M. McDaid, M. Weller, T. Weiss, H. Läubli, G. Hutter, Targeting the Siglec-sialic acid axis promotes antitumor immune responses in preclinical models of glioblastoma. *Sci. Transl. Med.* 15, eadf5302 (2023).
- F. Yang, D. Zhang, H. Jiang, J. Ye, L. Zhang, S. J. Bagley, J. Winkler, Y. Gong, Y. Fan, Small-molecule toosendanin reverses macrophage-mediated immunosuppression to overcome glioblastoma resistance to immunotherapy. Sci. Transl. Med. 15, eabq3558 (2023).
- M. H. Oh, I. H. Sun, L. Zhao, R. D. Leone, I. M. Sun, W. Xu, S. L. Collins, A. J. Tam, R. L. Blosser, C. H. Patel, J. M. Englert, M. L. Arwood, J. Wen, Y. Chan-Li, L. Tenora, P. Majer, R. Rais, B. S. Slusher, M. R. Horton, J. D. Powell, Targeting glutamine metabolism enhances tumor-specific immunity by modulating suppressive myeloid cells. *J. Clin. Invest.* 130, 3865–3884 (2020).
- S. M. Pyonteck, L. Akkari, A. J. Schuhmacher, R. L. Bowman, L. Sevenich, D. F. Quail,
   O. C. Olson, M. L. Quick, J. T. Huse, V. Teijeiro, M. Setty, C. S. Leslie, Y. Oei, A. Pedraza,
   J. Zhang, C. W. Brennan, J. C. Sutton, E. C. Holland, D. Daniel, J. A. Joyce, CSF-1R inhibition alters macrophage polarization and blocks glioma progression. *Nat. Med.* 19, 1264–1272 (2013).
- L. Akkari, R. L. Bowman, J. Tessier, F. Klemm, S. M. Handgraaf, M. de Groot, D. F. Quail, L. Tillard, J. Gadiot, J. T. Huse, D. Brandsma, J. Westerga, C. Watts, J. A. Joyce, Dynamic changes in glioma macrophage populations after radiotherapy reveal CSF-1R inhibition as a strategy to overcome resistance. Sci. Transl. Med. 12, eaaw7843 (2020).
- A. Subramanian, P. Tamayo, V. K. Mootha, S. Mukherjee, B. L. Ebert, M. A. Gillette, A. Paulovich, S. L. Pomeroy, T. R. Golub, E. S. Lander, J. P. Mesirov, Gene set enrichment analysis: A knowledge-based approach for interpreting genome-wide expression profiles. *Proc. Natl. Acad. Sci. U.S.A.* 102, 15545–15550 (2005).
- M. E. Ritchie, B. Phipson, D. Wu, Y. Hu, C. W. Law, W. Shi, G. K. Smyth, Limma powers differential expression analyses for RNA-sequencing and microarray studies. *Nucleic Acids Res.* 43, e47 (2015).
- G. K. Smyth, Linear models and empirical bayes methods for assessing differential expression in microarray experiments. Stat. Appl. Genet. Mol. Biol. 3, 10.2202/1544-6115.1027 (2004).
- M. E. Jönsson, R. Garza, Y. Sharma, R. Petri, E. Södersten, J. G. Johansson, P. A. Johansson, D. A. Atacho, K. Pircs, S. Madsen, D. Yudovich, R. Ramakrishnan, J. Holmberg, J. Larsson, P. Jern, J. Jakobsson, Activation of endogenous retroviruses during brain development causes an inflammatory response. *EMBO J.* 40, e106423 (2021).
- G. X. Y. Zheng, J. M. Terry, P. Belgrader, P. Ryvkin, Z. W. Bent, R. Wilson, S. B. Ziraldo, T. D. Wheeler, G. P. McDermott, J. Zhu, M. T. Gregory, J. Shuga, L. Montesclaros, J. G. Underwood, D. A. Masquelier, S. Y. Nishimura, M. Schnall-Levin, P. W. Wyatt, C. M. Hindson, R. Bharadwaj, A. Wong, K. D. Ness, L. W. Beppu, H. J. Deeg, C. McFarland, K. R. Loeb, W. J. Valente, N. G. Ericson, E. A. Stevens, J. P. Radich, T. S. Mikkelsen, B. J. Hindson, J. H. Bielas, Massively parallel digital transcriptional profiling of single cells. Nat. Commun. 8, 14049 (2017).
- R. Satija, J. A. Farrell, D. Gennert, A. F. Schier, A. Regev, Spatial reconstruction of single-cell gene expression data. *Nat. Biotechnol.* 33, 495–502 (2015).
- A. Fedorov, R. Beichel, J. Kalpathy-Cramer, J. Finet, J. C. Fillion-Robin, S. Pujol, C. Bauer,
   D. Jennings, F. Fennessy, M. Sonka, J. Buatti, S. Aylward, J. V. Miller, S. Pieper, R. Kikinis, 3D
   Slicer as an image computing platform for the Quantitative Imaging Network. *Magn. Reson. Imaging* 30, 1323–1341 (2012).
- D. Dejaco, C. Url, V. H. Schartinger, A. K. Haug, N. Fischer, D. Riedl, A. Posch,
   H. Riechelmann, G. Widmann, Approximation of head and neck cancer volumes in contrast enhanced CT. *Cancer Imaging* 15, 16 (2015).
- Y. Xie, T. Bergström, Y. Jiang, P. Johansson, V. D. Marinescu, N. Lindberg, A. Segerman, G. Wicher, M. Niklasson, S. Baskaran, S. Sreedharan, I. Everlien, M. Kastemar, A. Hermansson, L. Elfineh, S. Libard, E. C. Holland, G. Hesselager, I. Alafuzoff, B. Westermark, S. Nelander, K. Forsberg-Nilsson, L. Uhrbom, The Human Glioblastoma Cell Culture Resource: Validated cell models representing all molecular subtypes. EBioMedicine 2, 1351–1363 (2015).
- S. Offer, J. A. Menard, J. E. Pérez, K. G. De Oliveira, V. I. Chandran, M. C. Johansson, A. Bång-Rudenstam, P. Siesjö, A. Ebbesson, I. Hedenfalk, P. C. Sundgren, A. Darabi, M. Belting, Extracellular lipid loading augments hypoxic paracrine signaling and promotes glioma angiogenesis and macrophage infiltration. J. Exp. Clin. Cancer Res. 38, 241 (2019)

- J. Kasurinen, A novel fluorescent fatty acid, 5-methyl-BDY-3-dodecanoic acid, is a
  potential probe in lipid transport studies by incorporating selectively to lipid classes of
  BHK cells. *Biochem. Biophys. Res. Commun.* 187, 1594–1601 (1992).
- H. Li, P. N. Black, C. C. Dirusso, A live-cell high-throughput screening assay for identification of fatty acid uptake inhibitors. *Anal. Biochem.* 336, 11–19 (2005).
- T. de Neergaard, M. Sundwall, S. Wrighton, P. Nordenfelt, High-sensitivity assessment of phagocytosis by persistent association-based normalization. *J. Immunol.* 206, 214–224 (2021).
- V. I. Chandran, C. Welinder, A. S. Mansson, S. Offer, E. Freyhult, M. Pernemalm, S. M. Lund, S. Pedersen, J. Lehtio, G. Marko-Varga, M. C. Johansson, E. Englund, P. C. Sundgren, M. Belting, Ultrasensitive immunoprofiling of plasma extracellular vesicles identifies syndecan-1 as a potential tool for minimally invasive diagnosis of glioma. *Clin. Cancer Res.* 25, 3115–3127 (2019).
- V. Pantazopoulou, P. Jeannot, R. Rosberg, T. J. Berg, A. Pietras, Hypoxia-induced reactivity of tumor-associated astrocytes affects glioma cell properties. Cells 10, 613 (2021).
- G. Cattoretti, F. M. Bosiso, L. Marcelis, M. M. Bolognesi, "Multiple iterative labeling by antibody deposition (MILAN)" (Protocol Exchange, 25 September 2019).
- C. D. Gatenbee, A. M. Baker, S. Prabhakaran, O. Swinyard, R. J. C. Slebos, G. Mandal, E. Mulholland, N. Andor, A. Marusyk, S. Leedham, J. R. Conejo-Garcia, C. H. Chung, M. Robertson-Tessi, T. A. Graham, A. R. A. Anderson, Virtual alignment of pathology image series for multi-gigapixel whole slide images. *Nat. Commun.* 14, 4502 (2023).
- S. Kurup, T. J. M. Wijnhoven, G. J. Jenniskens, K. Kimata, H. Habuchi, J. P. Li, U. Lindahl, T. H. Van Kuppevelt, D. Spillmann, Characterization of anti-heparan sulfate phage display antibodies AO4B08 and HS4E4. J. Biol. Chem. 282. 21032–21042 (2007).
- H. Mi, A. Muruganujan, D. Ebert, X. Huang, P. D. Thomas, PANTHER version 14: More genomes, a new PANTHER GO-slim and improvements in enrichment analysis tools. *Nucleic Acids Res.* 47, D419–D426 (2019).
- S. Kotla, N. K. Singh, G. N. Rao, ROS via BTK-p300-STAT1-PPARγ signaling activation mediates cholesterol crystals-induced CD36 expression and foam cell formation. *Redox Biol.* 11, 350–364 (2017).
- A. Majdalawieh, L. Zhang, I. V. Fuki, D. J. Rader, H. S. Ro, Adipocyte enhancer-binding protein 1 is a potential novel atherogenic factor involved in macrophage cholesterol homeostasis and inflammation. *Proc. Natl. Acad. Sci. U.S.A.* 103, 2346–2351 (2006).
- S. O. Rahaman, D. J. Lennon, M. Febbraio, E. A. Podrez, S. L. Hazen, R. L. L. Silverstein, A CD36-dependent signaling cascade is necessary for macrophage foam cell formation. *Cell Metab.* 4, 211–221 (2006).
- A. W. Cohen, B. Razani, W. Schubert, T. M. Williams, X. B. Wang, P. Iyengar, D. L. Brasaemle, P. E. Scherer, M. P. Lisanti, Role of caveolin-1 in the modulation of lipolysis and lipid droplet formation. *Diabetes* 53, 1261–1270 (2004).
- J. Van Den Bossche, A. E. Neele, M. A. Hoeksema, M. P. J. De Winther, Macrophage polarization: The epigenetic point of view. Curr. Opin. Lipidol. 25, 367–373 (2014).
- Y. H. Goo, S. H. Son, P. B. Kreienberg, A. Paul, Novel lipid droplet-associated serine hydrolase regulates macrophage cholesterol mobilization. *Arterioscler. Thromb. Vasc. Biol.* 34, 386–396 (2014).
- V. R. Babaev, S. Fazio, L. A. Gleaves, K. J. Carter, C. F. Semenkovich, M. F. Linton, Macrophage lipoprotein lipase promotes foam cell formation and atherosclerosis in vivo. J. Clin. Invest. 103, 1697–1705 (1999).
- C. A. C. Freyre, P. C. Rauher, C. S. Ejsing, R. W. Klemm, MIGA2 links mitochondria, the ER, and lipid droplets and promotes de novo lipogenesis in adipocytes. *Mol. Cell* 76, 811–825.e14 (2019).
- C. Travelli, G. Colombo, S. Mola, A. A. Genazzani, C. Porta, NAMPT: A pleiotropic modulator of monocytes and macrophages. *Pharmacol. Res.* 135, 25–36 (2018).
- W. Xiao, C. Wang, K. Chen, T. Wang, J. Xing, X. Zhang, X. Wang, MiR-765 functions as a tumour suppressor and eliminates lipids in clear cell renal cell carcinoma by downregulating PLP2. EBioMedicine 51, 102622 (2020).
- X. C. Jiang, Y. Yu, The role of phospholipid transfer protein in the development of atherosclerosis. Curr. Atheroscler. Rep. 23, 9 (2021).
- C. Rae, S. A. Robertson, J. M. W. Taylor, A. Graham, Resistin induces lipolysis and re-esterification of triacylglycerol stores, and increases cholesteryl ester deposition, in human macrophages. FEBS Lett. 581, 4877–4883 (2007).
- V. L. King, J. Thompson, L. R. Tannock, Serum amyloid A in atherosclerosis. Curr. Opin. Lipidol. 22, 302–307 (2011).
- P. Chen, D. Zhao, J. Li, X. Liang, J. Li, A. Chang, V. K. Henry, Z. Lan, D. J. Spring, G. Rao,
   Y. A. Wang, R. A. DePinho, Symbiotic macrophage-glioma cell interactions reveal synthetic lethality in PTEN-null glioma. *Cancer Cell* 35, 868–884.e6 (2019).
- D. Zysset, B. Weber, S. Rihs, J. Brasseit, S. Freigang, C. Riether, Y. Banz, A. Cerwenka,
   C. Simillion, P. Marques-Vidal, A. F. Ochsenbein, L. Saurer, C. Mueller, TREM-1 links
   dyslipidemia to inflammation and lipid deposition in atherosclerosis. *Nat. Commun.* 7, 13151 (2016).
- N. Mor-Vaknin, A. Punturieri, K. Sitwala, D. M. Markovitz, Vimentin is secreted by activated macrophages. Nat. Cell Biol. 5, 59–63 (2003).

- S. Takahashi, Triglyceride rich lipoprotein-LPL-VLDL receptor and Lp(a)-VLDL receptor pathways for macrophage foam cell formation. J. Atheroscler. Thromb. 24, 552–559 (2017).
- D. An, F. Hao, F. Zhang, W. Kong, J. Chun, X. Xu, M. Z. Cui, CD14 is a key mediator of both lysophosphatidic acid and lipopolysaccharide induction of foam cell formation. *J. Biol. Chem.* 292, 14391–14400 (2017).
- E. González-Domínguez, R. Samaniego, J. L. Flores-Sevilla, S. F. Campos-Campos,
   G. Gómez-Campos, A. Salas, V. Campos-Peña, Á. L. Corbí, P. Sánchez-Mateos,
   C. Sánchez-Torres, CD163L1 and CLEC5A discriminate subsets of human resident and inflammatory macrophages in vivo. *J. Leukoc. Biol.* 98, 453–466 (2015).
- 115. J. L. Stöger, M. J. J. Gijbels, S. van der Velden, M. Manca, C. M. van der Loos, E. A. L. Biessen, M. J. A. P. Daemen, E. Lutgens, M. P. J. de Winther, Distribution of macrophage polarization markers in human atherosclerosis. *Atherosclerosis* 225, 461–468 (2012).
- 116. A. Roghanian, I. Teige, L. Mårtensson, K. L. Cox, M. Kovacek, A. Ljungars, J. Mattson, A. Sundberg, A. T. Vaughan, V. Shah, N. R. Smyth, B. Sheth, H. T. C. Chan, Z. C. Li, E. L. Williams, G. Manfredi, R. J. Oldham, C. I. Mockridge, S. A. James, L. N. Dahal, K. Hussain, B. Nilsson, J. S. Verbeek, G. Juliusson, M. Hansson, M. Jerkeman, P. W. M. Johnson, A. Davies, S. A. Beers, M. J. Glennie, B. Frendéus, M. S. Cragg, Antagonistic human FcyRIIB (CD32B) antibodies have anti-tumor activity and overcome resistance to antibody therapy in vivo. Cancer Cell 27, 473–488 (2015).
- 117. L. T. C. Vogelpoel, I. S. Hansen, T. Rispens, F. J. M. Muller, T. M. M. Van Capel, M. C. Turina, J. B. Vos, D. L. P. Baeten, M. L. Kapsenberg, E. C. De Jong, J. Den Dunnen, Fc gamma receptor-TLR cross-talk elicits pro-inflammatory cytokine production by human M2 macrophages. *Nat. Commun.* 5, 5444 (2014).
- S. Mukhopadhyay, E. Heinz, I. Porreca, K. Alasoo, A. Yeung, H. T. Yang, T. Schwerd, J. L. Forbester, C. Hale, C. A. Agu, Y. H. Choi, J. Rodrigues, M. Capitani, L. Jostins-Dean, D. C. Thomas, S. Travis, D. Gaffney, W. C. Skarnes, N. Thomson, H. H. Uhlig, G. Dougan, F. Powrie, Loss of IL-10 signaling in macrophages limits bacterial killing driven by prostaglandin E2. *J. Exp. Med.* 217, e20180649 (2020).
- 119. M. R. Alexander, C. W. Moehle, J. L. Johnson, Z. Yang, J. K. Lee, C. L. Jackson, G. K. Owens, Genetic inactivation of IL-1 signaling enhances atherosclerotic plaque instability and reduces outward vessel remodeling in advanced atherosclerosis in mice. J. Clin. Invest. 122, 70–79 (2012).
- Z. Liu, Z. Gao, B. Li, J. Li, Y. Ou, X. Yu, Z. Zhang, S. Liu, X. Fu, H. Jin, J. Wu, S. Sun, S. Sun,
   Q. Wu, Lipid-associated macrophages in the tumor-adipose microenvironment facilitate breast cancer progression. *Onco. Targets. Ther.* 11, 2085432 (2022).
- A. L. Bayliss, A. Sundararaman, C. Granet, H. Mellor, Raftlin is recruited by neuropilin-1 to the activated VEGFR2 complex to control proangiogenic signaling. *Angiogenesis* 23, 371–383 (2020).
- 122. K. Ma, S. Chen, X. Chen, C. Yang, J. Yang, \$100A10 is a new prognostic biomarker related to the malignant molecular features and immunosuppression process of adult gliomas. *World Neurosurg.* **165**, e650–e663 (2022).
- M. M. McCormick, F. Rahimi, Y. V. Bobryshev, K. Gaus, H. Zreiqat, H. Cai, R. S. A. Lord,
   C. L. Geczy, S100A8 and S100A9 in human arterial wall: Implications for atherogenesis.
   J. Biol. Chem. 280, 41521–41529 (2005).
- 124. S. Liu, K. Jin, Y. Hui, J. Fu, C. Jie, S. Feng, D. Reisman, Q. Wang, D. Fan, S. Sukumar, H. Chen, HOXB7 promotes malignant progression by activating the TGFβ signaling pathway. Cancer Res. 75, 709–719 (2015).
- 125. M. Segovia, S. Russo, M. Jeldres, Y. D. Mahmoud, V. Perez, M. Duhalde, P. Charnet, M. Rousset, S. Victoria, F. Veigas, C. Louvet, B. Vanhove, R. A. Floto, I. Anegon, M. C. Cuturi, M. R. Girotti, G. A. Rabinovich, M. Hill, Targeting TMEM176B enhances antitumor immunity and augments the efficacy of immune checkpoint blockers by unleashing inflammasome activation. *Cancer Cell* 35, 767–781.e6 (2019).
- B. Kaur, F. W. Khwaja, E. A. Severson, S. L. Matheny, D. J. Brat, E. G. Van Meir, Hypoxia and the hypoxia-inducible-factor pathway in glioma growth and angiogenesis. *Neuro-Oncology* 7, 134–153 (2005).
- W.-R. Ning, D. Jiang, X. C. Liu, Y.-F. Huang, Z.-P. Peng, Z.-Z. Jiang, T. Kang, S.-M. Zhuang, Y. Wu, L. Zheng, Carbonic anhydrase XII mediates the survival and prometastatic functions of macrophages in human hepatocellular carcinoma. *J. Clin. Invest.* 132, e153110 (2022).
- 128. Q. Zhang, S. Cheng, Y. Wang, M. Wang, Y. Lu, Z. Wen, Y. Ge, Q. Ma, Y. Chen, Y. Zhang, R. Cao, M. Li, W. Liu, B. Wang, Q. Wu, W. Jia, X. Wang, Interrogation of the microenvironmental landscape in spinal ependymomas reveals dual functions of tumor-associated macrophages. *Nat. Commun.* 12, 6867 (2021).
- M. C. Gage, N. Bécares, R. Louie, K. E. Waddington, Y. Zhang, T. H. Tittanegro,
   S. Rodríguez-Lorenzo, A. Jathanna, B. Pourcet, O. M. Pello, J. V. De la Rosa, A. Castrillo,
   I. Pineda-Torra, Disrupting lxrα phosphorylation promotes foxm1 expression and modulates atherosclerosis by inducing macrophage proliferation. *Proc. Natl. Acad. Sci. U.S.A.* 115, E6556–E6565 (2018).
- R. Du, K. V. Lu, C. Petritsch, P. Liu, R. Ganss, E. Passegué, H. Song, S. VandenBerg,
   R. S. Johnson, Z. Werb, G. Bergers, HIF1a induces the recruitment of bone marrow-

- derived vascular modulatory cells to regulate tumor angiogenesis and invasion. *Cancer Cell* **13**, 206–220 (2008).
- L. Sun, X. Zhang, Q. Song, L. Liu, E. Forbes, W. Tian, Z. Zhang, Y. Kang, H. Wang, J. B. Fleming, B. C. Pasche, W. Zhang, IGFBP2 promotes tumor progression by inducing alternative polarization of macrophages in pancreatic ductal adenocarcinoma through the STAT3 pathway. *Cancer Lett.* **500**, 132–146 (2021).
- 132. J. Guyon, I. Fernandez-Moncada, C. M. Larrieu, C. L. Bouchez, A. C. Pagano Zottola, J. Galvis, T. Chouleur, A. Burban, K. Joseph, V. M. Ravi, H. Espedal, G. V. Røsland, B. Daher, A. Barre, B. Dartigues, S. Karkar, J. Rudewicz, I. Romero-Garmendia, B. Klink, K. Grützmann, M. Derieppe, T. Molinié, N. Obad, C. Léon, G. Seano, H. Miletic, D. H. Heiland, G. Marsicano, M. Nikolski, R. Bjerkvig, A. Bikfalvi, T. Daubon, Lactate dehydrogenases promote glioblastoma growth and invasion via a metabolic symbiosis. EMBO Mol. Med. 14, e15343 (2022).
- A. Nishie, K. Masuda, M. Otsubo, T. Migita, M. Tsuyenosi, K. Kohno, T. Shuin, S. Naito, M. Ono, M. Kuwano, High expression of the Cap43 gene in infiltrating macrophages of human renal cell carcinomas. *Clin. Cancer Res.* 7, 2145–2151 (2001).
- 134. H. Semba, N. Takeda, T. Isagawa, Y. Sugiura, K. Honda, M. Wake, H. Miyazawa, Y. Yamaguchi, M. Miura, D. M. R. Jenkins, H. Choi, J. W. Kim, M. Asagiri, A. S. Cowburn, H. Abe, K. Soma, K. Koyama, M. Katoh, K. Sayama, N. Goda, R. S. Johnson, I. Manabe, R. Nagai, I. Komuro, HIF-1α-PDK1 axis-induced active glycolysis plays an essential role in macrophage migratory capacity. *Nat. Commun.* 7, 11635 (2016).
- 135. P. Bieniasz-Krzywiec, R. Martín-Pérez, M. Ehling, M. García-Caballero, S. Pinioti, S. Pretto, R. Kroes, C. Aldeni, M. Di Matteo, H. Prenen, M. V. Tribulatti, O. Campetella, A. Smeets, A. Noel, G. Floris, J. A. Van Ginderachter, M. Mazzone, Podoplanin-expressing macrophages promote lymphangiogenesis and lymphoinvasion in breast cancer. *Cell Metab.* 30, 917–936.e10 (2019).
- 136. T. Dai, S. R. Rosario, E. Katsuta, A. Sawant Dessai, E. J. Paterson, A. T. Novickis, E. Cortes Gomez, B. Zhu, S. Liu, H. Wang, S. I. Abrams, M. Seshadri, W. Bshara, S. Dasgupta, Hypoxic activation of PFKFB4 in breast tumor microenvironment shapes metabolic and cellular plasticity to accentuate metastatic competence. *Cell Rep.* 41, 111756 (2022).
- B. Yuan, Y. Xu, S. Zheng, PLOD1 acts as a tumor promoter in glioma via activation of the HSF1 signaling pathway. *Mol. Cell. Biochem.* 477, 549–557 (2022).
- F. Li, P. F. Egea, A. J. Vecchio, I. Asial, M. Gupta, J. Paulino, R. Bajaj, M. S. Dickinson,
   S. Ferguson-Miller, B. C. Monk, R. M. Stroud, Highlighting membrane protein structure and function: A celebration of the protein data bank. J. Biol. Chem. 296, 100557 (2021).
- K. A. Steen, H. Xu, D. A. Bernlohr, FABP4/aP2 regulates macrophage redox signaling and inflammasome activation via control of UCP2. Mol. Cell. Biol. 37, e00282–16 (2017).
- 140. T. Daubon, C. Léon, K. Clarke, L. Andrique, L. Salabert, E. Darbo, R. Pineau, S. Guérit, M. Maitre, S. Dedieu, A. Jeanne, S. Bailly, J. J. Feige, H. Miletic, M. Rossi, L. Bello, F. Falciani, R. Bjerkvig, A. Bikfalvi, Deciphering the complex role of thrombospondin-1 in glioblastoma development. *Nat. Commun.* 10, 1146 (2019).
- N. Osterberg, N. Ferrara, J. Vacher, S. Gaedicke, G. Niedermann, A. Weyerbrock,
   Doostkam, H. E. Schaefer, K. H. Plate, M. R. Machein, Decrease of VEGF-A in myeloid cells attenuates glioma progression and prolongs survival in an experimental glioma model. *Neuro-Oncology* 18, 939–949 (2016).
- 142. K. Zhang, R. Chai, Z. Zhao, K. Wang, J. Chen, T. Jiang, PATH-60. Bioinformatic profiling identifies the secreted glycoprotein Adamtsl4 to be a potential novel immune-related biomarker for primary glioblastoma. *Neuro-Oncology* 20 (Suppl. 6), vi171–vi172 (2018).
- 143. V. Ferrucci, F. Asadzadeh, F. Collina, R. Siciliano, A. Boccia, L. Marrone, D. Spano, M. Carotenuto, C. M. Chiarolla, D. De Martino, G. De Vita, A. Macrì, L. Dassi, J. Vandenbussche, N. Marino, M. Cantile, G. Paolella, F. D'Andrea, M. di Bonito, K. Gevaert, M. Zollo, Prune-1 drives polarization of tumor-associated macrophages (TAMs) within the lung metastatic niche in triple-negative breast cancer. iScience 24, 101938 (2021).
- P. Vijayagopal, S. R. Srinivasan, J. H. Xu, E. R. Dalferes, B. Radhakrishnamurthy,
   G. S. Berenson, Lipoprotein-proteoglycan complexes induce continued cholesteryl ester accumulation in foam cells from rabbit atherosclerotic lesions. J. Clin. Invest. 91, 1011–1018 (1993).
- M. C. Bosco, M. Puppo, C. Santangelo, L. Anfosso, U. Pfeffer, P. Fardin, F. Battaglia,
   L. Varesio, Hypoxia modifies the transcriptome of primary human monocytes:
   Modulation of novel immune-related genes and identification of cc-chemokine ligand
   20 as a new hypoxia-inducible gene. J. Immunol. 177, 1941–1955 (2006).
- 146. I. Halpert, U. I. Sires, J. D. Roby, S. Potter-Perigo, T. N. Wight, S. D. Shapiro, H. G. Welgus, S. A. Wickline, W. C. Parks, Matrilysin is expressed by lipid-laden macrophages at sites of potential rupture in atherosclerotic lesions and localizes to areas of versican deposition, a proteoglycan substrate for the enzyme. *Proc. Natl. Acad. Sci. U.S.A.* 93, 9748–9753 (1996)
- A. R. Nusrat, H. A. Chapman Jr., An autocrine role for urokinase in phorbol ester-mediated differentiation of myeloid cell lines. J. Clin. Invest. 87, 1091–1097 (1991).
- C. Pyke, N. Graem, E. Ralfkiaer, E. Rønne, G. Høyer-Hansen, N. Brünner, K. Danø, Receptor for urokinase is present in tumor-associated macrophages in ductal breast carcinoma. *Cancer Res.* 53, 1911–1915 (1993).

149. D. M. Gilkes, S. Bajpai, P. Chaturvedi, D. Wirtz, G. L. Semenza, Hypoxia-inducible factor 1 (HIF-1) promotes extracellular matrix remodeling under hypoxic conditions by inducing P4HA1, P4HA2, and PLOD2 expression in fibroblasts. J. Biol. Chem. 288, 10819–10829 (2013).

Acknowledgments: We thank all of the patients who contributed to this study. We are grateful to our colleagues at the Neurosurgery, Oncology, Pathology, and Radiology Departments for their important and continuous input. We thank B. Baldetorp for support with infrastructure, the BEA core facility, Karolinska Institute, for help with gene expression arrays, and I. Salonen for help with immunofluorescence staining. Funding: This work was supported by the Swedish Cancer Society grants CAN 23 2655 Pj 01 H and 23 2937 Pj 01 H (to M.B. and J.B.), the Swedish Research Council grant VR-MH 2023-02106 (to M.B.), the Swedish Childhood Cancer Foundation grants PR2023-0078 and PR2022-0117 (to M.B. and J.B.), the Fru Berta Kamprad Foundation (to M.B. and J.B.), the Sjöberg Foundation (to M.B. and J.B.), the Skåne University Hospital donation funds (to M.B.), the governmental funding of clinical research within the National Health Services, ALF (to M.B.), the European Union's Horizon 2020 COFUND Programme CanFaster 754299 (to M.B.), and a generous donation by V. Jeppsson (to M.B. and J.B.), Author contributions: V.G. and M.B. conceptualized the study. V.G., K.G.d.O., A.B.-R., S.O., M.C.-M., J.L., K.S., F.D., E. Gustafsson, J.A.M., R.G., J.J., T.d.N., P.C.S., P.N., and H.T. developed the

methodology. V.G., K.G.d.O., S.O., M.C.-M., A.B.-R., J.L., S.B., M.C.J., A.-S.M., F.D., E. Gustafsson, A.B., P.J., K.S., E. Gezelius, J.A.M., R.G., T.d.N., P.C.S., A.M.T., H.H., K.J.R., A.D., A.P., H.T., and M.B. performed the investigation. V.G., K.G.d.O., S.O., R.G., and M.B. wrote the original draft of the manuscript. V.G., K.G.d.O., S.O., M.C.-M., A.B.-R., J.L., S.B., M.C.J., A.-S.M., C.E., F.D., A.B., E.Gustafsson., J.A.M., R.G., J.J., T.d.N., P.C.S., P.N., A.D., K.F.-N., A.P., H.T., J.B., and M.B. reviewed and edited the manuscript. M.B. and J.B. acquired funding. C.E., K.F.N., and J.B. supplied resources. M.B. supervised the study. All authors have read and agreed to the submitted version of the manuscript. **Competing interests:** The authors declare that they have no competing interests. **Data and materials availability:** All data associated with this study are present in the paper or the Supplementary Materials. No proprietary materials not otherwise available were used in this study. The gene expression data generated in this manuscript have been deposited in the Gene Expression Omnibus (GEO) database under accession numbers GSE236478, GSE236494, GSE237673, GSE278136, and GSE267976.

Submitted 6 August 2023 Resubmitted 9 July 2024 Accepted 2 October 2024 Published 30 October 2024 10.1126/scitranslmed.adk1168